Journal of
Water & Climate Change

IWA PUBLISHING

Journal of Water and Climate Change Vol 13 No 8, 2847 doi: 10.2166/wcc.2022.202

Assessing the impact of climate change in the wheat–maize cropping system across the Huang–Huai–Hai Plain under future climate scenarios

Sana Zeeshan Shirazi, Xurong Mei*, Buchun Liu and Yuan Liu

Institute of Environment and Sustainable Development in Agriculture, Chinese Academy of Agricultural Sciences/National Engineering Laboratory of Efficient Crop Water Use and Disaster Reduction/Key Laboratory of Agricultural Environment, MARA, Beijing 100081, China
*Corresponding author. E-mail: meixurong@caas.cn

SZS, 0000-0003-4389-3358; XM, 0000-0002-5982-4093

ABSTRACT

General circulation models suggest that changes in climatic parameters will have an effect on food production globally. Therefore, this study assessed the impact of climate change on wheat–maize rotation areas in the Huang–Huai–Hai Plain (3H Plain). The projections generated suggest an increase in precipitation during the wheat growth period (WGP) by 1.33–4.16% (2.6–8.3 mm) and 3.13–8.16% (6.2–18.0 mm) under RCP4.5 and RCP8.5, respectively, relative to the base period (1981–2016). Across the 3H Plain, the mean temperature during the WGP is projected to increase between 1.17–1.21 and 1.17–1.28 °C under RCP4.5 and RCP8.5, respectively. The projections during the maize growth period (MGP) indicate an increase in the temperature between 1.29–1.92 and 1.84–2.08 °C under RCP4.5 and RCP8.5, respectively. During the MGP, precipitation is also projected to increase by 7.41–9.73% (33.6–45.1 mm) and 6.63–14.78% (29.8–72.7 mm) under RCP4.5 and RCP8.5 scenarios, respectively. For each 1% change in climatic factors, the comprehensive effect on yield was projected to be 0.65 and 0.58% for wheat and −1.08 and −1.11% for maize, under RCP4.5 and RCP8.5, respectively, when other factors were kept constant. The change in water resources will be insignificant during the WGP and more pronounced during the MGP. The study provides an overview of changes in meteorological parameters and scientific evidence for climate change adaptation in the wheat–maize cropping system.

Key words: climate change, Huang–Huai–Hai Plain, statistical downscaling, summer maize, winter wheat, yield

HIGHLIGHTS

- The temperature and precipitation are projected to increase under RCP4.5 and RCP8.5 for both winter wheat and summer maize.
- The change in climate variables is projected to be beneficial for wheat yield under both emission scenarios with the highest increase in Shandong and parts of Henan.
- The summer maize yields are estimated to decrease due to increased temperature, particularly in the north 3H region.

GRAPHICAL ABSTRACT

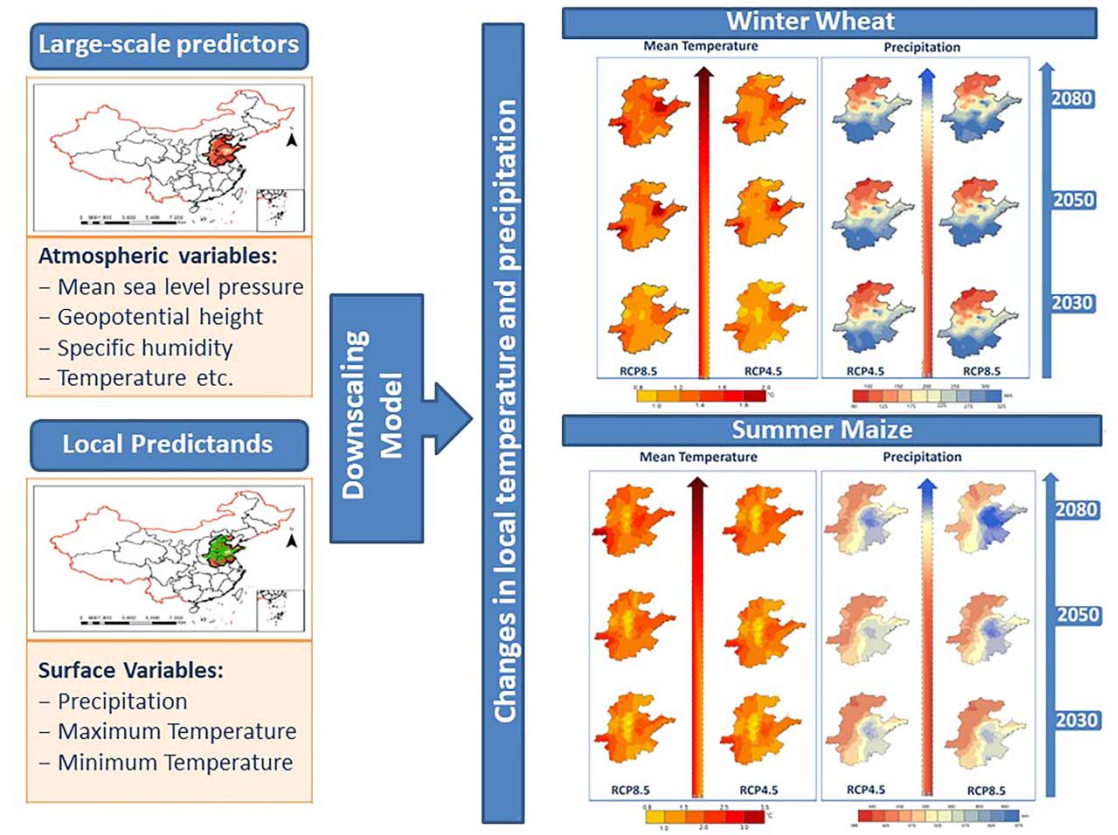

1. INTRODUCTION

The increase in greenhouse gas emissions due to anthropogenic activities is no doubt an undisputable contributor to global climate change. The International Panel on Climate Change (IPCC) issued a warning in 2018 about anthropogenic warming, indicating an increase of 1.5 °C in global temperature between the years 2032–2052, without major cuts in carbon dioxide (CO_2) emissions (IPCC 2018). Agriculture and food systems are likely to be most affected by climate change and variability because of their high dependence and sensitivity to climatic conditions (Motha & Baier 2005). There are also concerns that climate change may lead to a loss in water and consequently will negatively affect crop yields of staple cereals such as wheat, rice, and maize to varying degrees depending on regions and latitudes. The IPCC special report 'Climate Change and Land' (IPCC 2019) has reported adverse impact of observed climate change on wheat and maize yields in many lower-latitude regions in recent decades, unlike higher latitudes where yields have generally increased. Maize and wheat projection statistics at the global level confirm this trend, showing a yield increase for wheat and maize at high latitude and a decrease at low latitude by the end of the century (Rosenzweig *et al.* 2014).

Agriculture in China, particularly Northeast China, has been one of the most sensitive areas to climate change in the country during the last five decades (Lv *et al.* 2015). It is projected that climate change will have a significant impact on China's agriculture, as with each degree-Celsius increase in global mean temperature, the loss in yield is estimated to be about 8.0% for maize and 2.6% for wheat for the period 2071–2100 in comparison with the 1981–2010 baseline. Considering the global projections, it is important to analyze the impact of climate change on wheat and maize yield in the Huang–Huai–Hai (3H) Plain, which is one-sixth (23.3 million ha) of China's total cultivated area (134.86 million ha).

Climatic parameters, such as temperature and precipitation, have a direct impact on crop yield. The rising temperatures can also affect crop production negatively due to shortened growing seasons and decreased photosynthetic accumulation in plants (Lobell & Field 2007). Another effect of heat stress is the increased transpiration resulting in higher plant water demand. Similarly, changes in rainfall patterns also affect yield, particularly in rain-fed cropping areas. The comprehensive

effect of climate change on plant productivity understandably depends on the interaction of all these factors. Therefore, to ensure suitable site-specific adaptation measures in the 3H Plain, it is critical to quantitatively estimate the impact of changes in all climatic variables on agricultural production and to map the spatiotemporal variability of crop yield to empower the resource managers with the information to ensure best management strategies.

Several studies in China have conducted statistical downscaling and employed process-based crop models to study the impact of climate change on crop yield and change in irrigation demand (Tang *et al.* 2018; Liu *et al.* 2021). The relationship between climate variability and crop yield has been confirmed in many studies using statistical approaches. To simulate crop yield using process-based models, climate inputs are required at a finer spatial resolution, and therefore, global or regional scale projections are not adequate. Therefore, crop models in combination with downscaled future climate data from global circulation models (GCMs) are an important tool to assess the crop response to various climate scenarios, irrigation regimes, and agronomic management conditions.

Even though a lot of research has been done in China related to statistical downscaling and the impact of change in climatic variables on meteorological patterns, the impact of climatic changes has been least studied in crop rotation systems, particularly wheat and maize. Therefore, there is a need to quantify and assess the impact of climate change on yield to further expand the knowledge for climate adaptation potential in agricultural applications. The goal of this study was to understand the impact of climate change in the wheat–maize cropping system at 90 study locations in the 3H Plain. The specific objectives of the study were to (1) produce downscaled climate data for the selected study sites; (2) explore the change in temperature and precipitation during winter wheat and summer maize crop growth periods, and (3) understand the impact of climatic changes on the wheat and maize yield in the 3H Plain. The impact of climate change results has been produced for medium (RCP4.5) and high (RCP8.5) emission scenarios (2016–2030, 2031–2070, and 2071–2099). To simulate the crop yields, the AquaCrop Model was used for historical and future timelines.

2. MATERIAL AND METHODS

2.1. Study area

This study focused on the 3H Plain, which lies within latitudes 31 °14′N to 40 °25′N and longitudes 112 °33′E to 120 °17′E (Li *et al.* 2017), and covers approximately 350,500 km^2. The 3H Plain includes the area of five provinces (Shandong, Hebei, parts of Henan, and northeastern parts of Anhui and Jiangsu) and two municipalities (Beijing and Tianjin) (Wang *et al.* 2018). The croplands in this region constitute around one-sixth (23.3 million ha) of China's total cultivated area (134.86 million ha) and contribute more than 70% of the winter wheat and 30% of the summer maize production to China's total harvest (Li *et al.* 2017). The 3H Plain is an alluvial plain formed by the intermittent flooding of the Huang He (Yellow River), Huai He, and Hai He rivers. The climate of the region falls in the East Asian Temperate Monsoon Climate zone (Li *et al.* 2017), with an annual mean temperature and precipitation varying between 8 and 15 °C and from 430 to 1,390 mm, respectively, which decreases gradually from the southeast to the northwest. The region follows a wheat (early October to early June of the subsequent year) and maize (mid-June to late September) crop rotation system (Wang *et al.* 2018). Since summer (June–September) receives 60–80% of the annual precipitation in the region, abundant water is available for the summer maize but severe water shortages are experienced during the winter wheat season. A total of 90 study sites (32 in Hebei, 32 in Shandong, 13 in Henan, 4 in Jiangsu, and 3 each in Beijing, Tianjin, and Anhui) were selected for this study (Figure 1).

2.2. Climate data

The data used in this study included meteorological data (1978–2018) and GCM data (2016–2100). The meteorological data used in this study were the China Meteorological Forcing Dataset (CMFD) developed by the National Tibetan Plateau Data Center (TPDC), Beijing, China. This data had a spatial and temporal resolution of 0.1° and 3 h, respectively, which were updated and evaluated regularly by the TPDC (He *et al.* 2020). The dataset was released in 2019 and made through a combination of remote sensing products, a reanalysis dataset, and *in situ* observation data at weather stations. The daily mean, maximum, and minimum temperatures and precipitation data for the period of 1979–2018 were used to generate future climate predictions. The data from the TPDC climate forcing product were extracted using China Meteorological Administration (CMA) ground weather observation station locations issued in its list available at the CMA website (http://data.cma.cn/). The TPDC data have shown a high correlation with the data available from the ground observation stations of the CMA and can be used for a wide range of applications at a finer resolution.

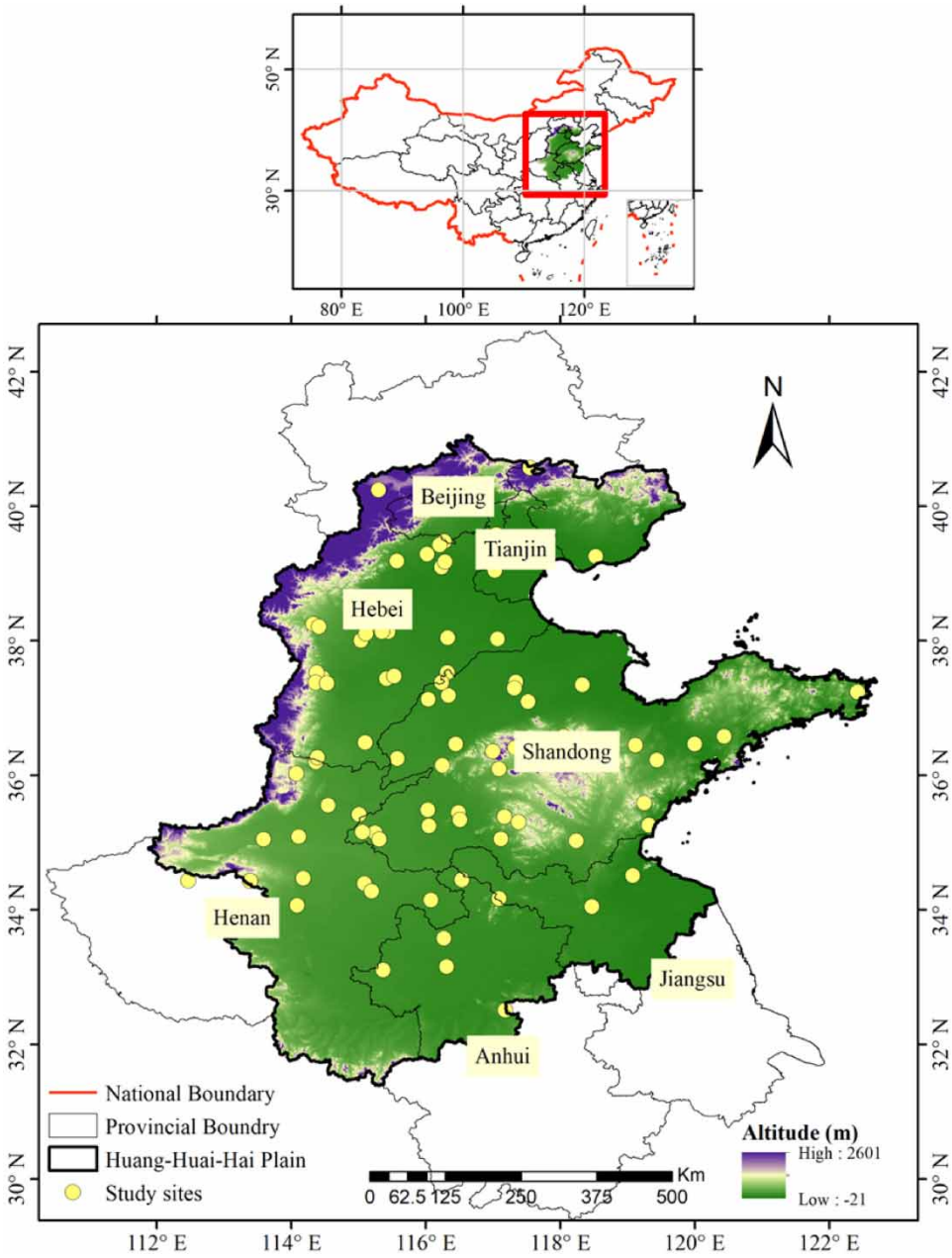

Figure 1 | Location map of study sites in the 3H Plain for which downscaled products (precipitation and maximum and minimum temperatures) were produced and crop growth simulations were carried out.

The second-generation Canadian Earth System Model (CanESM2) consists of the physical coupled atmosphere-ocean model CanCM4 coupled to a terrestrial carbon model (CTEM), and an ocean carbon model (CMOC) was used for the period 2016–2100. CanESM2 predictor's data were developed by the Canadian Centre for Climate Modeling and Analysis (CCCma) of Environment and Climate Change Canada representing the IPCC Fifth Assessment Report (AR5). The predictor data were available in the 128×64 grid cells covering the global domain according to the T42 Gaussian grid at the uniform horizontal resolution of 2.8125° along the longitude and the latitude (available at http://climate-scenarios.canada.ca). The National Centers for Environmental Prediction (NCEP) reanalysis climatic data were used to identify appropriate atmospheric variables and calibrate and validate the model predictions in historical time, and CanESM2 climatic data were used to generate RCP4.5 and RCP8.5 scenario datasets.

2.3. Statistical downscaling model

Statistical Downscaling Model (SDSM) 4.2, open-source software, which is a decision support tool to assess the local climate change impacts using a robust statistical downscaling technique, was used in this study. The SDSM supports the creation of multiple, low-cost, and site-specific scenarios from daily weather variables, such as maximum and minimum temperatures, precipitation, and humidity under current and future regional climate forcing. The SDSM also produces a range of statistical parameters such as variances, frequencies of extremes, and spell lengths. The statistical software provides the support for predictor (weather station historical data) pre-screening, calibration, diagnostic testing, statistical analysis, and graphing of the climate data. The SDSM has been applied in various geographical settings across the globe to produce high-resolution climate change future scenarios including various parts of China. In this study, the SDSM was used to downscale the climate data of each station by establishing the statistical relationship between predictors and predictands using multi-linear regression and stochastic bias correction techniques.

2.4. Data processing

The data processing was divided into five steps, namely, predictor selection, the calibration of daily weather predictands using selected GCM predictors, the generation of model predictions for the historical period (1979–2018), the validation of the model predictions with observed data, and the generation of the future downscaled weather series based on the best-identified predictors. Before any data processing, quality control of observed data for all weather variables was done for each study location and ensured that there were no data gaps.

First, the empirical relationship between the CMFD predictands (e.g. temperature and minimum and maximum temperatures) and the NCEP predictors (e.g. specific humidity, precipitation, geopotential height, and mean sea level pressure) was identified, which varied over space and time. NCEP predictors showed a high correlation with the observed historical weather data; therefore, they were used for calibration and validation of the SDSM output results.

Suitable NECP predictors (from Table 1) were first selected based on the strength of their empirical relationship with predictands (temperature and precipitation). Correlation matrix, partial correlation, and *p*-value statistics were used to define the strength of the relationship between predictor and predictand, which varied over space and time. The probable predictors displaying significant correlation at 95% confidence level with the observed data were selected. Furthermore, the exploration of predictor and predictand relationship was also carried out using scatter plot analysis. In this study, weather data for 90 locations were screened for three weather variables (precipitation and maximum and minimum temperatures). Therefore, 26 large-scale predictors were analyzed more than 7,020 times (90 stations $\times$ 26 large-scale predictors $\times$ 3 predictands).

Table 1 | List of 26 large-scale predictors and their corresponding variable names

No.	Short variable name	Predictor names	No.	Short variable name	Predictor names
1	mslpgl	Mean sea level pressure	14	p5zh	500 hPa Divergence of true wind
2	p1_f	1,000 hPa Wind speed	15	p850	850 hPa Geopotential
3	p1_u	1,000 hPa Zonal wind component	16	p8_f	850 hPa Wind speed
4	p1_v	1,000 hPa Meridional wind component	17	p8_u	850 hPa Zonal wind component
5	p1_z	1,000 hPa Relative vorticity of true wind	18	p8_v	850 hPa Meridional wind component
6	p1th	1,000 hPa Wind direction	19	p8_z	850 hPa Relative vorticity of true wind
7	p1zh	1,000 hPa Divergence of true wind	20	p8th	850 hPa Wind direction
8	p500	500 hPa Geopotential	21	p8zh	850 hPa Divergence of true wind
9	p5_f	500 hPa Wind speed	22	Prcp	Total precipitation
10	p5_u	500 hPa Zonal wind component	23	s500	500 hPa Specific humidity
11	p5_v	500 hPa Meridional wind component	24	s850	850 hPa Specific humidity
12	p5_z	500 hPa Relative vorticity of true wind	25	shum	1,000 hPa Specific humidity
13	p5th	500 hPa Wind direction	26	temp	Air temperature at 2 m

The second step was the calibration of the SDSM using the selected predictors for a specific predictand at each of the study locations (Figure 1). For each predictand, the model was calibrated under an unconditional process for maximum and minimum temperatures and a conditional process for precipitation on a monthly scale. Unconditional processes follow as a direct link between large-scale predictands and local-scale predictors, while conditional processes depend on an intermediate variable between predictands and predictors. Therefore, the temperature was modeled as unconditional and precipitation as a conditional process.

In this study, the downscaling process was carried out for all 90 study locations (Figure 1), and 20 ensembles were produced for each variable and location. The mean of 20 ensembles has been taken by writing the code in R for further use in the study (Supplementary material S1). Ideally, the model is calibrated using part of the observed available data, withholding the remainder of the data for independent model validation. In this study, the observed data were available for the period 1979–2018 (40 years). Half of the data (1979–1998) were used for calibration and the remainder was held for independent model validation.

In the third step, for the validation period, the weather generator produced ensembles of synthetic daily weather series, given observed predictor variables and regression model weights produced in the calibration. As a fourth step, performance analysis of the observed and modeled data was carried out through analyzing the unconditional and conditional statistics of both observed and model datasets. The data for both periods were plotted on line and bar graphs to compare and decide if the model predicted accurate results. The results were compared on a monthly basis to have a better understanding. Bias correction was then applied to correct the model bias. In the SDSM, stochastic techniques are included to improve the model performance in reproducing the observed data by artificially inflating the variance of the model output. In the final step, after checking the validation results, the calibrated model was used to generate future scenarios using the CanESM2 predictors available under RCP4.5, and RCP8.5 from 2016 to 2099. Figure 2 shows the downscaling workflow of the SDSM used in this study.

2.5. Use of crop model and projected potential yield

For the historical period (2008–2016), the growth of winter wheat and summer maize was simulated based on the soil data, field management, and crop phenology data obtained from the published literature for the Xiaotangshan County in Beijing (Jin *et al.* 2014); Luancheng County in Hebei (Umair *et al.* 2017); Xinxiang County in Henan (Tang *et al.* 2018); Taian County in Shandong (Bian *et al.* 2016) and Guangde County in Anhui (Chen *et al.* 2016). The literature also provided sufficient

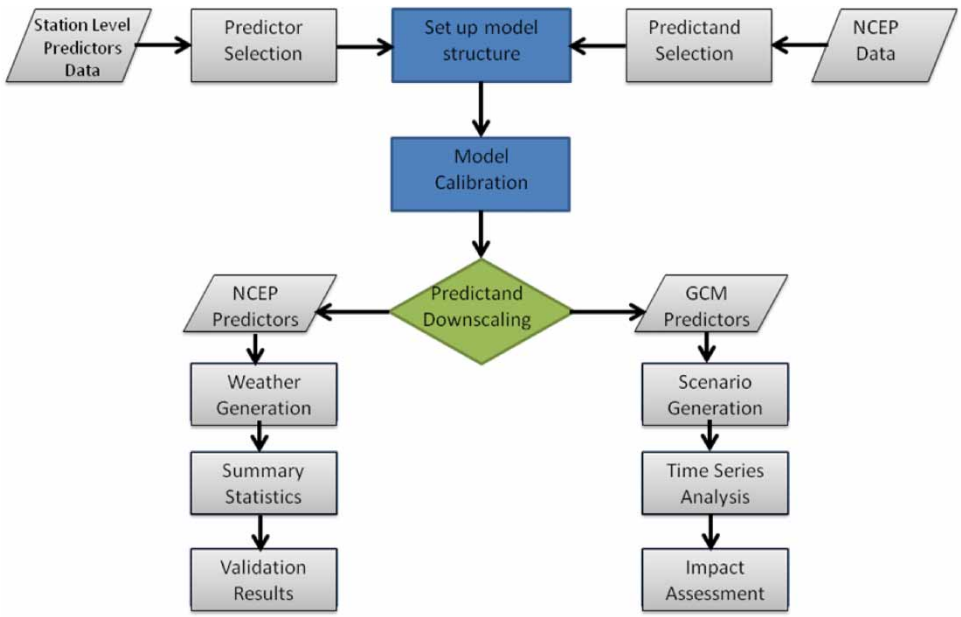

Figure 2 | Schematic workflow of the SDSM to generate daily climate data.

information regarding sowing and harvesting dates, irrigation timing, amounts, and other management measures needed for calibration and validation of the AquaCrop Model (Shirazi *et al.* 2021) (Table 2). The calibration process also involved adjusting the non-conservative parameters, which included initial canopy cover CC_o (%), canopy growth coefficient (CGC), coefficients for triggering water stress affecting leaf expansion, and canopy senescence until a close match between observed and simulated yield and biomass was obtained. The performance was evaluated by comparing the simulated grain yield results and the observed grain yield data obtained from the literature under full irrigation for both winter wheat and summer maize during the 2011–2016 period. The AquaCrop model was then used to simulate the potential yield of winter wheat and summer maize using downscaled data for future scenarios for the period 2016–2099.

2.6. Projected climate and yield data analysis for the wheat and maize growth period

The projected changes in the weather variables (precipitation and maximum and minimum temperatures) and potential yield for both future climate scenarios (RCP4.5 and RCP8.5) were analyzed for three timelines: 2030s (2016–2040), 2050s (2041–2070), and 2080s (2071–2099). Under both RCP4.5 and RCP8.5 scenarios, the increase in precipitation and mean, maximum, and minimum temperatures was projected relative to the base period (1981–2016). The period from early October to mid-June is considered as the winter wheat growth period (WGP) and mid-June to the end of September as the summer maize growth period (MGP) as this cycle is widely practiced in wheat and maize rotation areas across the 3H Plain, but in the lower regions of the 3H Plain, the maize harvest is around mid-September. In this study, we considered wheat and maize crop cycles based on actual agronomic conditions that varied between different provinces in the 3H Plain. The ordinary Kriging method was used to analyze the changes by generating spatial distribution maps for all variables in ArcGIS-V10.1.

2.7. Evaluation of model performance

The monthly model results for precipitation and maximum and minimum temperatures were evaluated within the SDSM model as it offers conditional and unconditional statistical methods to assess the results by comparing observed and model outputs. For further evaluation, the statistical indices chosen in this study include the coefficient of determination (R^2), root mean square error (RMSE), mean absolute error (MAE), percent deviation, and index of agreement (d) using Equations (1)–(5). The performance of the model outputs from both the SDSM and the AquaCrop models was evaluated using the above-mentioned indices. The evaluation results of the SDSM model for all 90 locations have been provided in

Table 2 | Parameters used in the AquaCrop model to simulate winter wheat and summer maize cropping during the calibration and validation period

Province	Beijing	Hebei	Henan	Shandong	Anhui	Hebei
County	Xiaotangshan	Luancheng	Xinxiang	Taian	Guangde	Wuqiao
Crop type	WW	WW	WW	WW	WW	SM
Cultivar type	Jingdong8	Kenong199	Bainong207	Jimai22	Yangmai20	Zhengdan958
Sowing date	25 Sep 2011	10 Oct 2012	18 Oct 2015	7 Oct 2014	28 Oct 2014	16 June 2015
Harvest date	9 June 2012	11 June 2013	5 June 2016	9 June 2015	3 June 2015	4 Oct 2015
Calibration year	2011–2012	2012–2013	2015–2016	2014–2015	2014–2015	2015
Validation year	2008–2009	2011–2012	–	2013–2014	–	2014, 2013
Plants (ha)	333,000	250,000	250,000	250,000	250,000	75,000
Harvest index	46	48	52	48	41	53
Physiological maturity (GDD)	2,198	1,953	2,327	2,498	2,135	1,925
Irrigation (mm)	273	369	240	120	–	75
Reference literature	Jin *et al.* (2014)	Umair *et al.* (2017)	Tang *et al.* (2018)	Bian *et al.* (2016)	Chen *et al.* (2016)	Wang *et al.* (2018)

Supplementary material (S2).

$$R^2 = \left[\frac{\sum_{i=1}^{N} (O_i - \bar{O})(P_i - \bar{P})}{\sqrt{\sum_{i=1}^{N} (O_i - \bar{O})^2 \cdot \sum_{i=1}^{N} (P_i - \bar{P})^2}} \right]^2 \quad (1)$$

$$\text{RMSE} = \sqrt{\frac{1}{n} \sum_{i=1}^{n} (P_i - O_i)^2} \quad (2)$$

$$\text{Percent deviation} = (\text{Predicted} - \text{Observed}) \times \frac{100}{\text{Observed}} \quad (3)$$

$$\text{MAE} = \frac{1}{n} \sum_{i=1}^{n} |P_i - O_i| \quad (4)$$

$$d = 1 - \frac{\sum_{i=1}^{n} (P_i - O_i)^2}{\sum_{i=1}^{n} (|P_i - \bar{O}| + |O_i - \bar{O}|)^2} \quad (5)$$

where P_i indicates predicted values, O_i indicates observed values, and $\bar{O}$ and $\bar{P}$ indicate the mean of observed and predicted data, respectively.

For R^2, the results closer to 1 indicate a perfect fit. For RMSE, a result close to zero indicates a better fit of the model. MAE measures the absolute value of the difference between the simulated value and the observed value. The values can range from 0 to infinite. Lower values represent a better agreement between predicted and observed values. Index of Agreement (IOA) measures how well the model produced the estimates, the value of 1 indicates a perfect match between observed and predicted and 0 indicates no agreement at all.

We also used multiple regression analysis to examine the relationship between forecasted yield and climate predictors downscaled for the future time period. The strength of the relationship between dependent (yield) and independent (precipitation and maximum and minimum temperatures) variables was determined, and the importance of each of the climatic predictors to the relationship was assessed with the effect of other predictors statistically eliminated. Using linear regression, we tried to understand the change in forecasted yield, given one-unit change in precipitation and temperature. We specified the formula for multiple linear regressions as followed in Equation (6). We also linearized the equation by taking the logarithm of both sides as shown in Equation (7).

$$y = \beta_0 + \beta_1 X_1 + \beta_2 X_2 + \beta_3 X_3 + \varepsilon \quad (6)$$

$$\ln(y) = \beta_0 + \beta_1 \ln(X_1) + \beta_2 \ln(X_2) + \beta_3 \ln(X_3) + \varepsilon \quad (7)$$

where β_0 is the intercept when all X are set to zero, β_1 to β_3 are regression coefficients for the climatic parameters and ε is the model error. We denoted X_1 to precipitation, X_2 to maximum temperature, and X_3 to minimum temperature.

3. RESULTS

3.1. Technical validation and evaluation

3.1.1. Statistical Downscaling Model

The monthly observed and modeled results were compared in the SDSM model by generating summary statistics such as monthly mean, maximum, 95th percentile, and variance. An explanatory example of observed and modeled output comparison of monthly mean, maximum, and 95th percentile during the validation period for three representative sites (selected based on their weather conditions representative of other study sites) has been provided in Figure 3, indicating the modeling precision for all 12 months. However, over- and underestimations are evident in modeling the monthly maximum values of

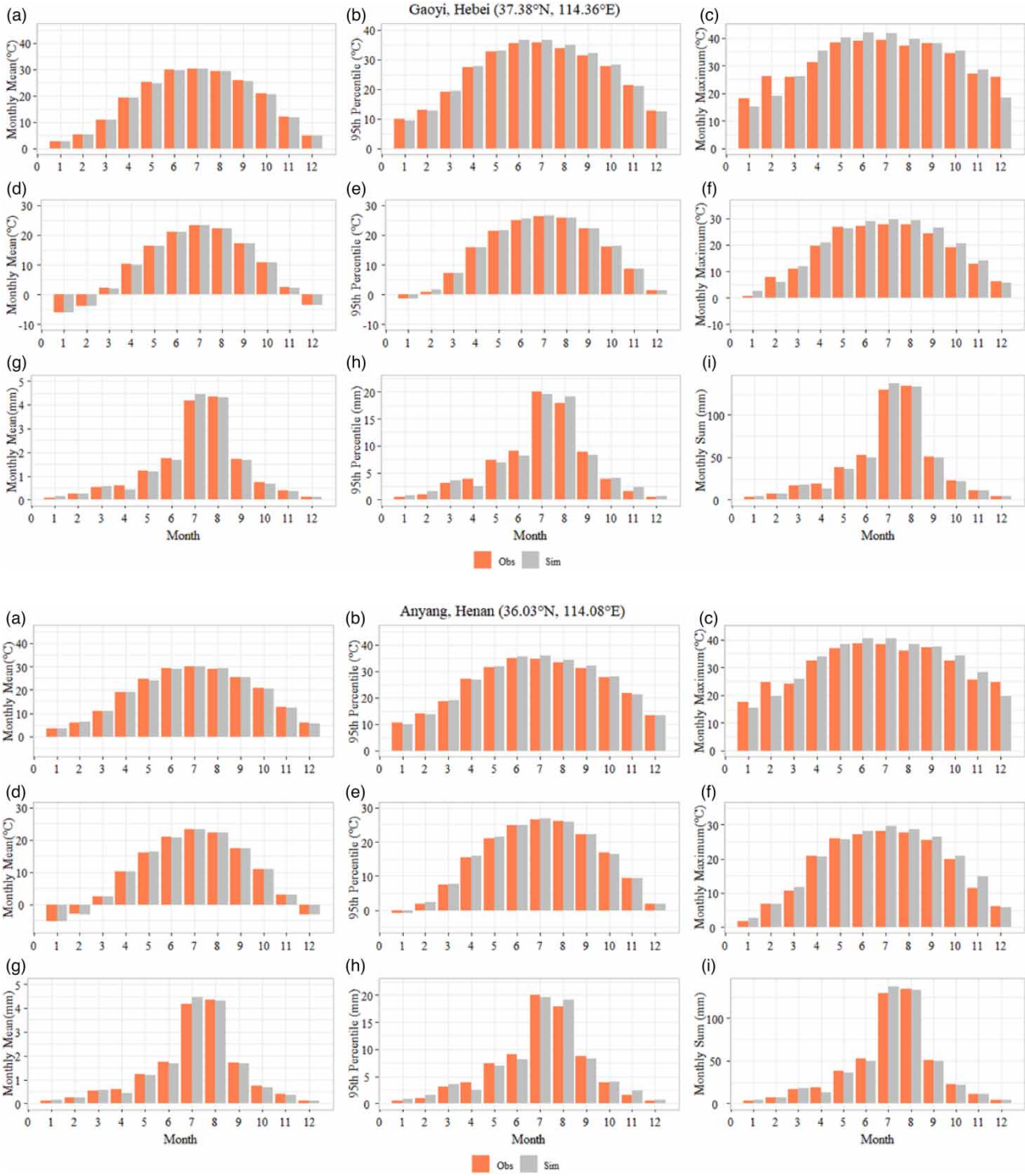

Figure 3 | Observed and modeled output comparison of monthly mean, maximum, and 95th percentile of maximum temperature (a-c), minimum temperature (d-f), and precipitation (mm) (g-i) for three representative sites in the 3H Plain. (*Continued*).

both maximum and minimum temperatures, which can be due to the presence of outliers in the observed data. The results show that the model accuracy is higher for maximum and minimum temperatures as compared to precipitation, mainly because local temperatures are largely interconnected with regional climate forcing, whereas precipitation is affected by

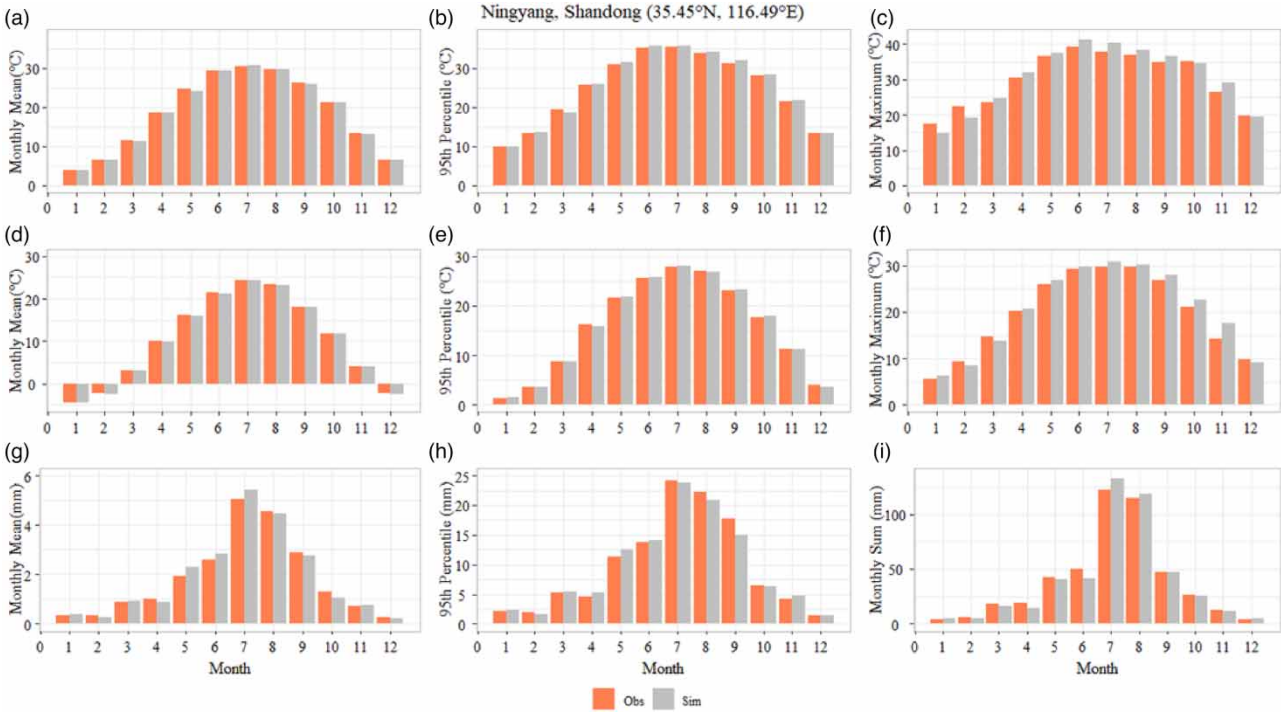

Figure 3 | (*Continued*).

many local factors such as prevailing winds, seasonal winds, presence of mountains, and mean sea level pressure at a given site.

The model results of the bias-corrected weather data for the validation period (1999–2018) were evaluated based on the R^2, RMSE, MAE, percent bias, and IA. For the mean monthly sum of the precipitation, R^2 (0.925–0.993), RMSE (0.237–1.007), MAE (0.237–1.007), percent bias ($\pm$3.7%), and IA (0.954–0.996) were in the acceptable range at 0.05 significance level, which indicated that the model had the feature of high fitting precision.

The R^2 (0.993–0.999), RMSE (0.355–1.110), MAE (0.264–0.967), percent bias ($-$0.1 to $-$1.007%), and IA (0.996–0.999) for the mean monthly maximum temperature also showed model results fitting with higher accuracy with the observed data. The statistical evaluation results for the mean monthly minimum temperature were as follows: R^2 (0.997–0.999), RMSE (0.223–2.120), MAE (0.163–1.823), percent bias ($-$3 to $-$4%), and IA (0.990–0.999) indicate the results range for all study locations. The correlation between mean monthly observed and simulated results of precipitation and maximum and minimum temperatures has also been provided separately in Figure 4 at the monthly level for the validation period (1999–2018). The results of R^2, RMSE, MAE, percent bias, and IA used to evaluate the model performance have been provided in the Supplementary material (S2) for all study locations and selected variables.

3.1.2. The AquaCrop model

Crop yields were simulated for both winter wheat and summer maize using agronomic practices mentioned in Table 2 (section 2.5), which are widely used across the 3H Plain. For all locations of winter wheat, the percent deviation of grain yield estimates from the observed data was between 0.42 and $-$11.0% for both the calibration and validation stages. Similarly, for summer maize, the percent deviation of grain yield estimates from the observed data varied between $-$1.44 and $-$8.90% for both calibration and validation stages, respectively. The RMSE between the observed and simulated grain yield was 0.12–1.01 t ha^{-1} for winter wheat, while it was 0.50–0.53 t ha^{-1} for summer maize. Overall, the calibration results show a reasonably close match between the observed and those simulated by the model for both winter wheat and summer maize.

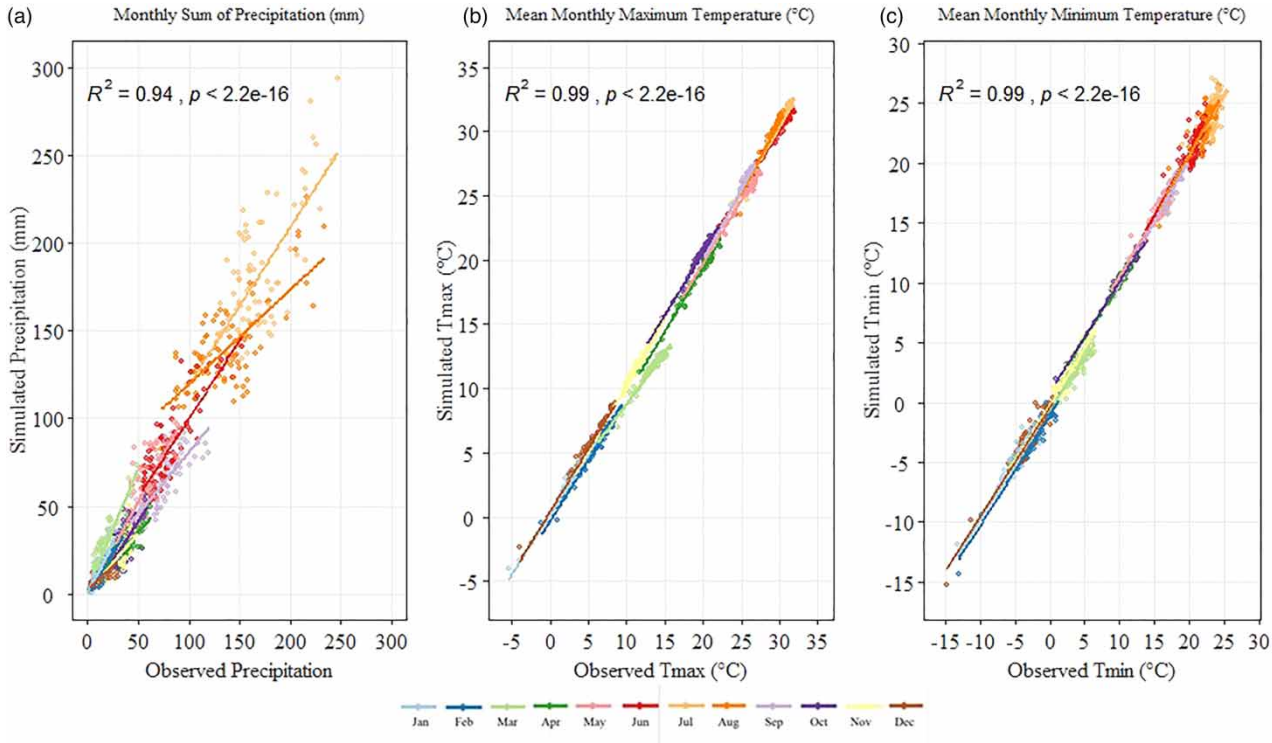

Figure 4 | Correlation between mean monthly observed and simulated results of climatic variables, i.e., Precipitation, Maximum temperature (Tmax), and minimum temperature (Tmin) for the validation period (1999-2018) at all 90 study sites. (Each data point represents a mean monthly value of one station location.)

3.2. Change in temperature and precipitation trends

Figure 5(a) and 5(b) shows the change in precipitation (mm), and Figure 5(c) and 5(d) shows the increase in mean temperature (°C) projected for the 2030s (2016–2040), 2050s (2041–2070), and 2080s (2071–2099) relative to the baseline period of 1981–2016 for the medium emission scenario (RCP4.5) and the high-emission scenario (RCP8.5) for winter WGP and summer MGP, respectively.

The mean temperature during the winter WGP is projected to increase by 0.90–1.85 °C under RCP4.5 and 0.90–2.34 °C under RCP8.5 across the 3H Plain from 2016 to 2099, relative to the baseline period (1981–2016). The mean temperature during the summer MGP will increase by 0.90–3.13 °C under RCP4.5 and 0.90–3.58 °C under RCP8.5 across the 3H Plain from 2016 to 2099, relative to the baseline period. Parts of Shandong and Henan provinces will experience the most warming during both crop growing periods (Figures 6 and 7). In terms of the whole study area, the mean temperature is projected to experience a rise of about 1.25 °C for RCP4.5 and 1.35 °C for RCP8.5 during the winter WGP and 1.85 °C for RCP4.5 and 1.92 °C for RCP8.5 during the summer MGP for the period 2016–2099 with significant spatial variations.

The change in mean monthly maximum and minimum temperatures has been provided in Figure 8(a) and 8(b) for winter WGP and summer MGP, respectively, for the 2030s, 2050s, and 2080s under RCP4.5 and RCP8.5 compared to the base period. The difference in the changes under RCP4.5 is relatively lower as compared to RCP8.5. A significant increase is projected in the mean monthly temperature from October to December and May to September during both crop growth periods. The maximum temperature and minimum temperature will increase significantly from June to September in the summer MGP and October to December during the winter WGP. However, the monthly mean maximum temperature from January to April in the winter WGP will not increase significantly. The month of June is the maturity and harvest for winter wheat and planting of summer maize. The greatest increase in the maximum temperature (2.0 °C) is anticipated in the month of October, while the greatest increase in the minimum temperature (2.07 °C) is projected in the month of June during the winter WGP under the RCP8.5 scenario in the 2080s. During the summer MGP, the months of August and September are projected to face greater warming in the 2080s under RCP8.5.

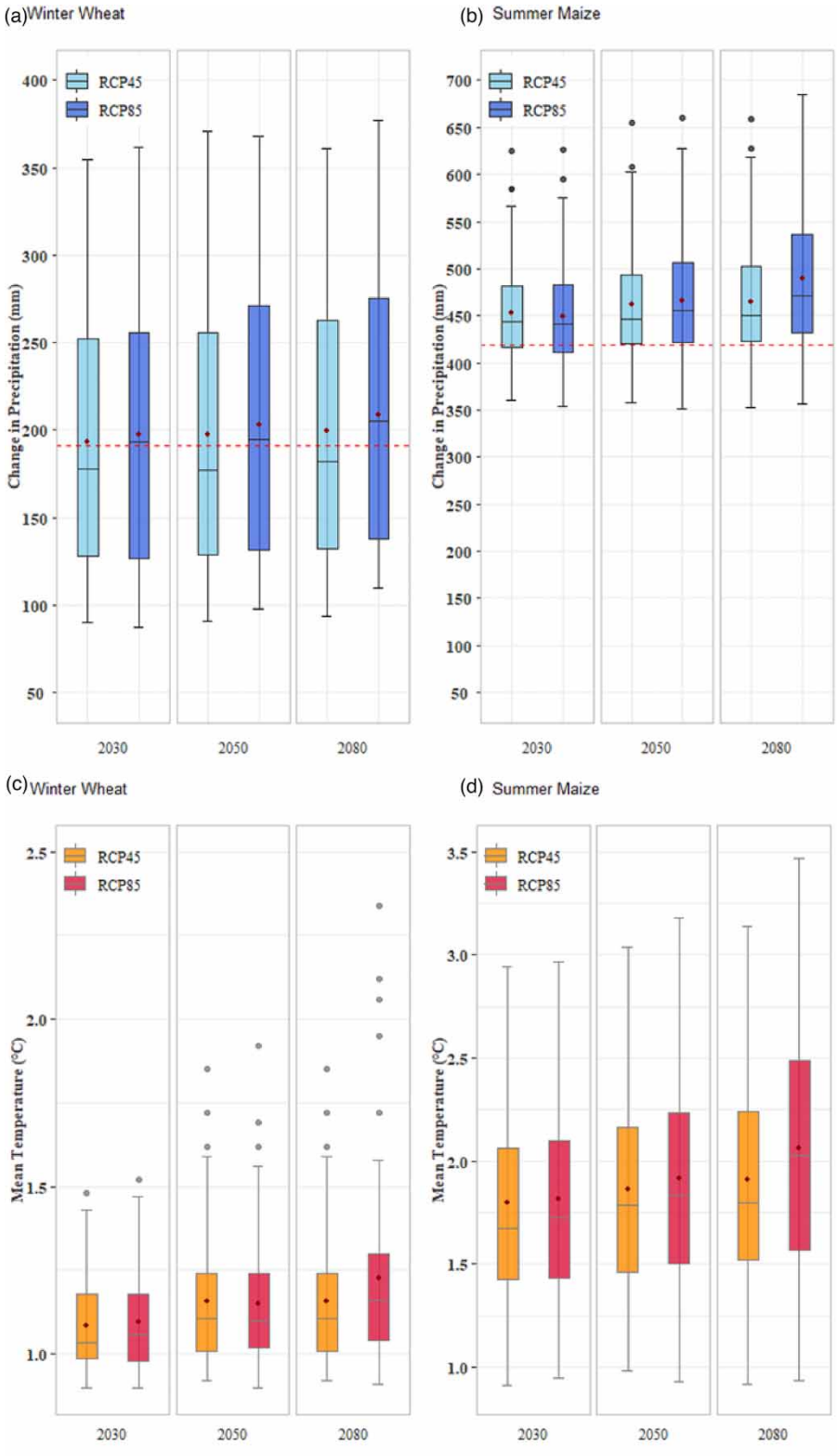

Figure 5 | Projected changes in the sum of the precipitation (mm) (a,b) and mean temperature (°C) (c,d) during the winter WGP and the summer MGP for the scenario period 2030s, 2050s, and 2080s under RCP4.5 and RCP8.5, relative to the mean for the base period (red dashed line). Please refer to the online version of this paper to see this figure in colour: http://dx.doi.org/10.2166/wcc.2022.202.

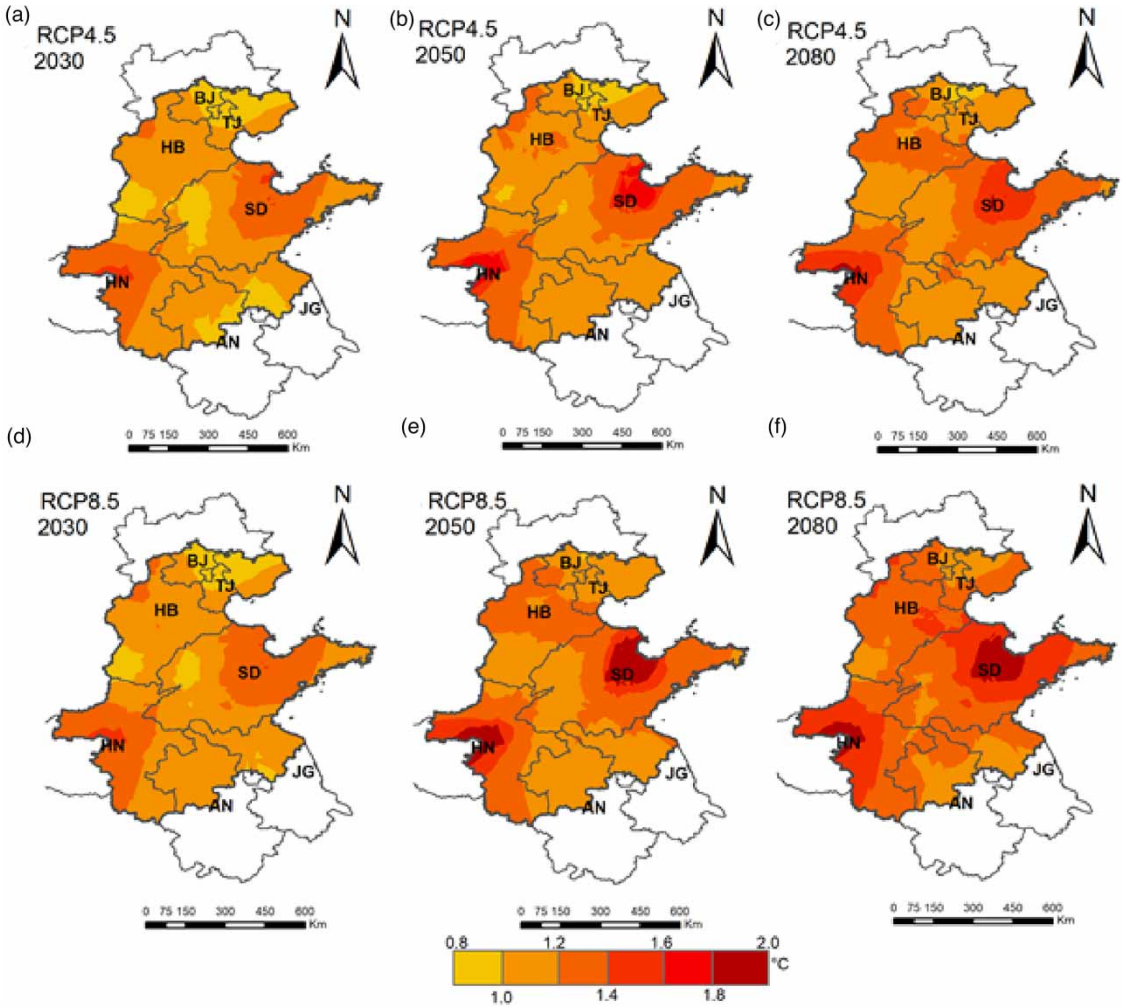

Figure 6 | Centigrade (°C) increase during the winter WGP from 2016 to 2099, relative to the base period (1981–2016) across the 3H Plain in 2030s, 2050s, and 2080s under RCP4.5 (a–c) and RCP8.5 (d–f), respectively.

The changes in precipitation results shown in Figures 9 and 10 also suggest that there will be an increasing trend in the precipitation, with summer maize receiving more increase as compared to winter wheat. Shandong province is projected to experience more precipitation during both crop growth periods. In terms of the whole study area, during the winter WGP, the increase in precipitation is 1.33, 3.19, and 4.17% in the 2030s, 2050s, and 2080s, respectively, for RCP4.5 and 3.13, 6.13, and 8.61% in the 2030s, 2050s, and 2080s, respectively, for RCP8.5, relative to the base period (191 mm) (Figure 5(a)). For the summer MGP, the increase in precipitation is 7.41, 9.21, and 9.73% in the 2030s, 2050s, and 2080s, respectively, for RCP4.5 and 6.63, 10.19, and 14.78% in the 2030s, 2050s, and 2080s, respectively, for RCP8.5, relative to the base period (419 mm) (Figure 5(b)). The precipitation increment is higher under RCP8.5 as compared to RCP4.5.

3.3. Impact of temperature and precipitation variables on wheat and maize yield

To better understand the functional relationship between independent variables (precipitation and maximum and minimum temperatures) and dependent variable (yield), we conducted multiple regression analysis to know the strength of the relationship (Table 3) and the projected change in yield with the change in climatic factors. The analysis was carried out to better understand the relevant contribution of each of the independent variables to the total variance for yield. The results in Table 3 show the strength of relationship between the wheat and maize yield and independent climatic variables and their significance under both RCP4.5 and RCP8.5. The relationship of winter wheat was significant ($p \leq 0.05$) with precipitation and maximum and minimum temperatures under both RCPs for all time periods. For summer maize, the negative relationship of yield is prominently significant ($p \leq 0.05$) with minimum and maximum temperatures under both RCP scenarios.

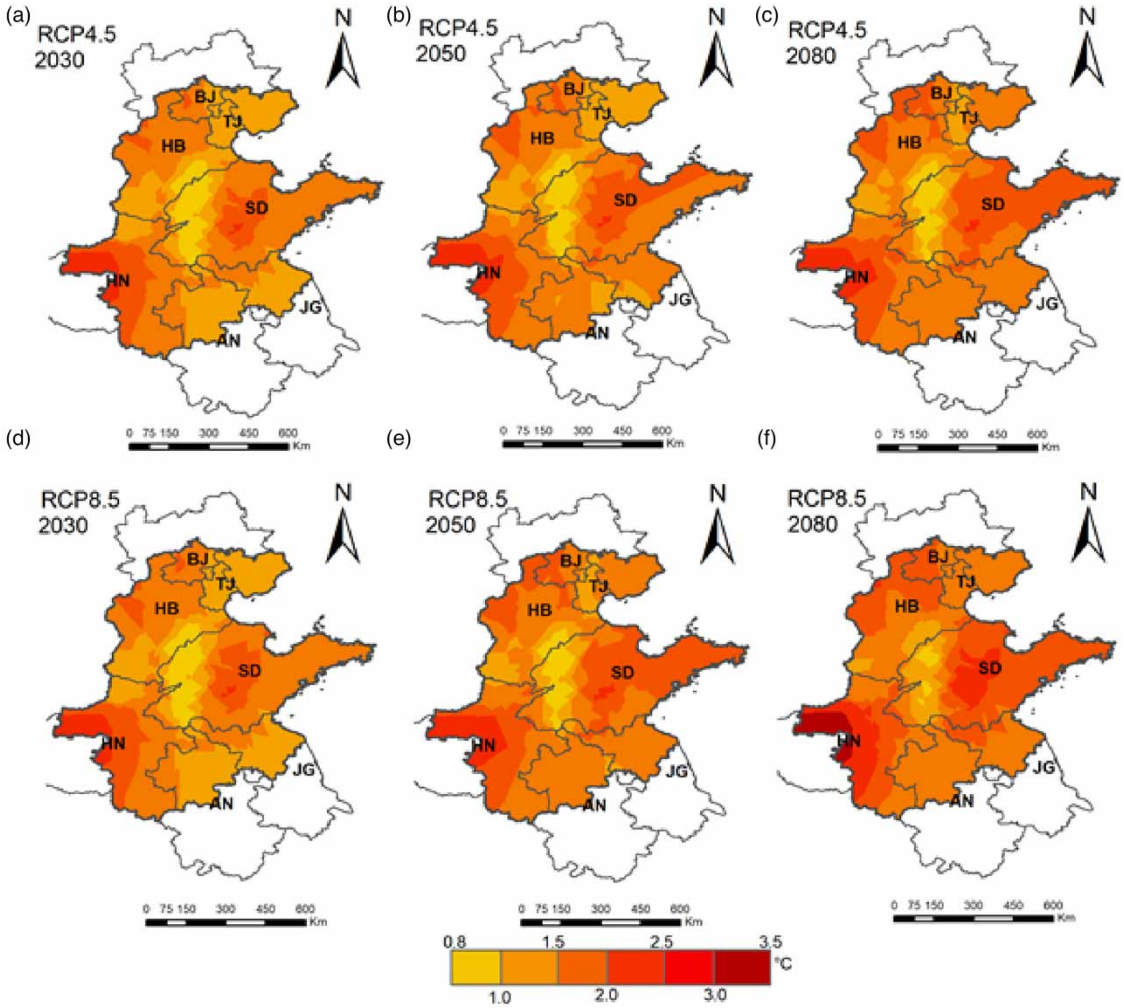

Figure 7 | Centigrade (°C) increase during the summer MGP from 2016 to 2099, relative to the base period (1981–2016) across the 3H Plain in the 2030s, 2050s, and 2080s under RCP4.5 (a–c) and RCP8.5 (d–f), respectively.

The summary of the entire regression model can be seen in Table 4, which shows that a significant amount of variation in yield can be explained by the change in our independent climatic variables.

The regression coefficients were produced to understand the effect of change in independent variables on yield under RCP4.5 and RCP8.5 (Table 5). Finally, to better understand the perspective, we used the climate estimates (precipitation and maximum and minimum temperatures) under RCP4.5 and RCP8.5, and analyzed the effects of changes on yield separately and combined for all time periods (Table 6). For winter wheat, irrigation is widely applied and has a significant effect on crop yield; therefore, we included irrigation as part of the analysis.

For winter wheat, an increase of every 1% in precipitation is contributing to increase the yield by 0.68%, while the increase in maximum temperature gives a decrease of 0.72% of yield under RCP4.5. The increase in 1% minimum temperature is increasing the wheat yield by 0.39% under RCP4.5, while the increase is merely 0.13% under RCP8.5, which indicates that the inhibitory effect of increased maximum temperature is more pronounced as compared to the minimum temperature. With every 1% increase in irrigation, the increase in wheat yield is 0.30% under RCP4.5 and 0.20% under RCP8.5. In terms of the comprehensive effect of 1% change in climatic variables and irrigation is beneficial to the wheat yield by an increase of 0.65% under RCP4.5 and 0.54% under RCP8.5.

We used estimates of climate change to obtain the effects on the projected yield under RCP4.5 and RCP8.5 (Table 6) for both winter wheat and summer maize. For winter wheat, an increase in the maximum temperature gives a decrease in yield,

Figure 8 | Mean monthly changes in the projected maximum temperature (a) and the minimum temperature (b) with respect to the base period under RCP4.5 and RCP8.5 scenarios during the winter WGP and the summer MGP.

while an increase in precipitation and minimum temperature increases the yield under RCP4.5 for the whole study area. A similar effect has been observed under RCP8.5, but this increase is relatively less as compared to RCP4.5. The comprehensive effect of an increase in all climatic variables will benefit wheat yield with an increase under both RCP scenarios. The positive effect of the increase in climatic variables will increase gradually from the 2030s to 2080s, and the study area experiences a substantial increase in precipitation counteracting the negative effect of rising temperatures during the winter WGP.

For summer maize, the increase in precipitation and maximum and minimum temperatures is projected to decrease yields under RCP4.5. The effect of increased precipitation under RCP8.5 becomes beneficial to increase the yields, but the increased maximum and minimum temperatures are projected to decrease the yields. The comprehensive effect of all variables is projected to decrease maize yields under both RCP scenarios. The highest decrease in maize yields was projected in the 2080s under both RCP scenarios.

When changes in climatic parameters (precipitation and maximum and minimum temperatures) were taken into account, the spatial distribution of winter wheat yield tends to increase across all RCP scenarios and timelines (Figure 11). It is projected that climatic parameters will contribute to increase the wheat yield particularly in Shandong province and parts of Henan province that are also expected to have more precipitation under RCP4.5 and RCP8.5 (Figure 9). The precipitation patterns in the north 3H region will remain similar to present conditions, resulting in a slight increase in yield mainly due to an increase in the minimum temperature.

Figure 12 shows the impact of change in climatic parameters on summer maize yield. The effect of increased temperature during the summer MGP is attributing to the decrease in maize yields. Under RCP4.5, the decrease in maize yields has been projected in Beijing, Tianjin and central Hebei with the highest decrease in the 2080s. Under RCP8.5, the decrease in maize yields is much more evident in the 2050s and 2080s, and all parts of Hebei, Beijing, Tianjin and Shandong are estimated to experience the effect of warming on maize yields up to 0.5 t ha^{-1} relative to the base period.

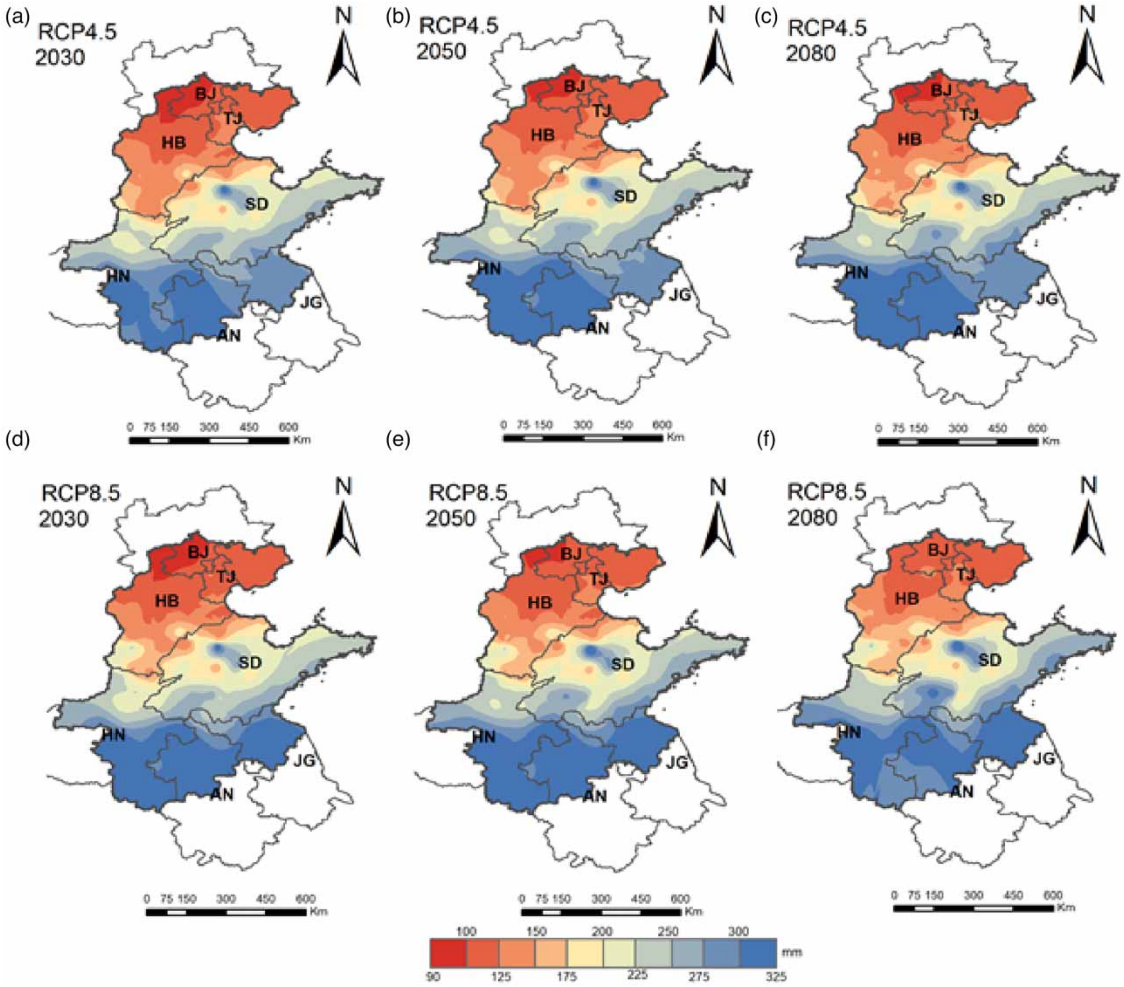

Figure 9 | Change in precipitation during the winter WGP from 2016 to 2099 relative to the base period (1981–2016) across the 3H Plain in the 2030s, 2050s, and 2080s under RCP4.5 (a–c) and RCP8.5 (d–f), respectively.

Figure 13 shows the impact of climate change on winter wheat potential yield under RCP4.5 (Figure 13(a)–13(d)) and RCP8.5 (Figure 13(e)–13(h)) across the 3H Plain on an annual basis. A comprehensive effect of the three parameters on the winter wheat yield is net positive in both scenarios; however, the yield demonstrates a stronger positive response under the RCP4.5 scenario (Figure 13(d)) as compared to RCP8.5 (Figure 13(h)). Considering individual parameters such as precipitation and minimum temperature can be observed to have a positive impact on yield, unlike maximum temperature, which shows a negative correlation with yield under both RCP4.5 and RCP8.5. Effects of precipitation can be observed to be more pronounced in the RCP8.5 scenario as compared to RCP4.5 (Figure 13(a) and 13(e)).

Figure 14 shows the impact of climate change on summer maize potential yield under RCP4.5 (Figure 14(a)–14(d)) and RCP8.5 across the 3H Plain on an annual basis. A comprehensive effect of the three parameters on the summer maize yield is net negative, unlike their effect observed on winter wheat in both scenarios; however, the yield demonstrates a stronger negative response under the RCP8.5 scenario (Figure 14(d)) as compared to RCP4.5 (Figure 14(h)). Similarly, focusing on the individual, precipitation, and maximum and minimum temperatures all impact the yield for summer maize negatively in both RCP4.5 and RCP8.5 scenarios. The only exception observed is the effect of precipitation during RCP8.5 (Figure 14(e)), which has a slight positive impact on summer maize yield.

The increase in temperatures has a direct effect on the reduction in growing seasons of the crops. Figure 15 shows the impact of increased temperatures on the length of cropping season of winter wheat and summer maize. During the base

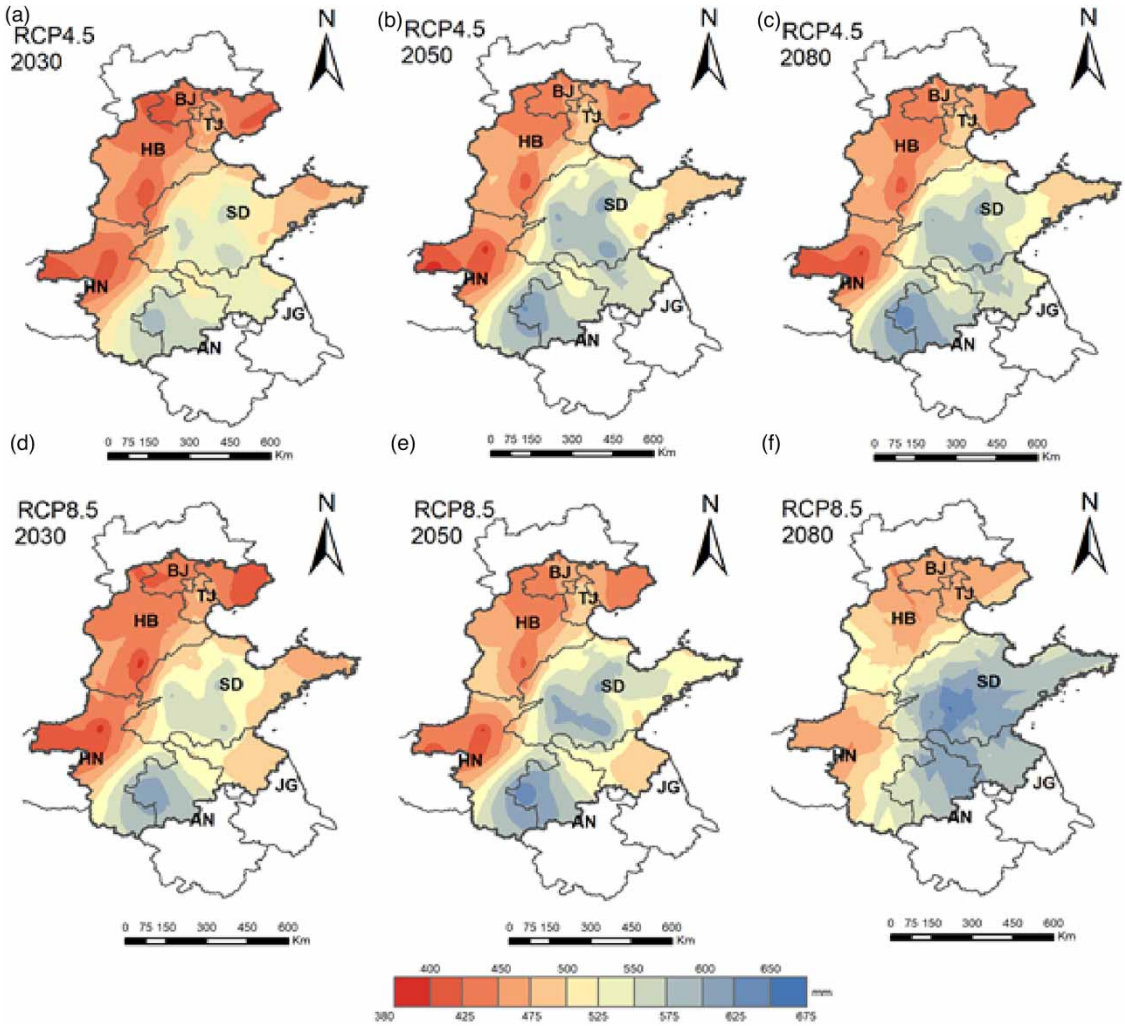

Figure 10 | Change in precipitation during the summer MGP from 2016 to 2099 relative to the base period (1981–2016) across the 3H Plain in the 2030s, 2050s, and 2080s under RCP4.5 (a–c) and RCP8.5 (d–f), respectively.

Table 3 | Pearson correlations among dependent (yield) and independent variables (precipitation and maximum and minimum temperatures)

			Prec.		Max. temp.		Min. temp.	
Crop	**RCP**	**Scenario period**	***r***	**Sig.**	***r***	**Sig.**	***r***	**Sig.**
Winter wheat	RCP4.5	Sc. 2030	0.777	0.000	0.319	0.002	0.492	0.000
		Sc. 2050	0.774	0.000	0.314	0.002	0.487	0.000
		Sc. 2080	0.780	0.000	0.318	0.002	0.482	0.000
	RCP8.5	Sc. 2030	0.723	0.000	0.349	0.001	0.450	0.000
		Sc. 2050	0.717	0.000	0.324	0.001	0.430	0.000
		Sc. 2080	0.714	0.000	0.323	0.002	0.394	0.000
Summer maize	RCP4.5	Sc. 2030	0.147	0.098	−0.183	0.053	−0.904	0.000
		Sc. 2050	0.187	0.050	−0.173	0.063	−0.903	0.000
		Sc. 2080	0.172	0.065	−0.147	0.098	−0.901	0.000
	RCP8.5	Sc. 2030	0.168	0.068	−0.140	0.109	−0.870	0.000
		Sc. 2050	0.209	0.031	−0.146	0.099	−0.861	0.000
		Sc. 2080	0.203	0.036	−0.155	0.084	−0.871	0.000

Table 4 | Summary of the entire regression model for the yield

Crop	RCP	Scenario period	R	R^2	Adj. R^2	SE	Sig.
Winter wheat	RCP4.5	Sc. 2030	0.890	0.793	0.782	0.040	0.000
		Sc. 2050	0.881	0.776	.0764	0.042	0.000
		Sc. 2080	0.878	0.771	0.759	0.042	0.000
	RCP8.5	Sc. 2030	0.779	0.607	0.586	0.054	0.000
		Sc. 2050	0.800	0.640	0.622	0.052	0.000
		Sc. 2080	0.801	0.641	0.622	0.053	0.000
Summer maize	RCP4.5	Sc. 2030	0.908	0.824	0.817	0.010	0.000
		Sc. 2050	0.908	0.824	0.817	0.010	0.000
		Sc. 2080	0.904	0.818	0.811	0.010	0.000
	RCP8.5	Sc. 2030	0.873	0.762	0.752	0.011	0.000
		Sc. 2050	0.865	0.748	0.738	0.011	0.000
		Sc. 2080	0.864	0.747	0.737	0.011	0.000

Table 5 | Predicted regression coefficients for winter wheat (WW) and summer maize (SM) yield with future climate under RCP4.5 and RCP8.5

	Every 1% incr. in Prec.		Every 1% incr. in max. temp.		Every 1% incr. in min. temp.		Every 1% incr. in irrigation		Comprehensive effect (%)	
Crop	RCP4.5	RCP8.5	RCP4.5	RCP8.5	RCP4.5	RCP8.5	RCP4.5	RCP8.5	RCP4.5	RCP8.5
WW	0.68	0.58	−0.72	−0.37	0.39	0.13	0.30	0.20	0.65	0.54
SM	−0.01	0.01	−0.19	−0.22	−0.85	−0.92	–	–	−1.08	−1.11

Table 6 | Effects of climate change on yield for different scenarios under RCP4.5 and RCP8.5

		Effects of precipitation (%)		Effects of max. temp. (%)		Effects of min. temp. (%)		Comprehensive effect (%)	
Crop	Scenario period	RCP4.5	RCP8.5	RCP4.5	RCP8.5	RCP4.5	RCP8.5	RCP4.5	RCP8.5
Winter wheat	Sc. 2030	0.91	1.58	−4.22	−1.32	3.95	0.31	0.64	0.56
	Sc. 2050	2.14	3.55	−3.97	−2.55	3.94	1.41	2.10	2.42
	Sc. 2080	2.81	5.68	−3.88	−2.81	3.54	3.14	2.47	6.01
	All	1.95	3.60	−4.02	−2.23	3.81	1.62	1.74	3.00
Summer maize	Sc. 2030	−0.09	0.03	−0.53	−0.70	−3.32	−3.69	−3.93	−4.36
	Sc. 2050	−0.08	0.12	−0.67	−0.88	−3.60	−4.56	−4.36	−5.32
	Sc. 2080	−0.11	0.09	−0.81	−0.86	−4.13	−5.75	−5.05	−6.52
	All	−0.09	0.08	−0.67	−0.81	−3.68	−4.67	−4.44	−5.40

period, the length of winter wheat crop cycle was 242 days, while the summer maize cycle was 110 days. The length of the winter wheat crop cycle has decreased 1.8–2.6 and 5.0–6.5 days under RCP4.5 and RCP8.5, respectively, relative to the base period. The length of summer maize crop cycle has decreased 2.8–5.6 and 5.2–9.6 days under RCP4.5 and RCP8.5, respectively, relative to the base period.

4. DISCUSSION

It is noted that there are large uncertainties in projections generated by various models that stem from various sources, such as downscaling models, methods and bias correction, emission scenarios, and time period considered in the study. Since agricultural applications require higher precision to avoid the accumulation of error in the simulated yield from crop models, these uncertainties make use of these downscaled products challenging in agricultural applications. Greater consensus

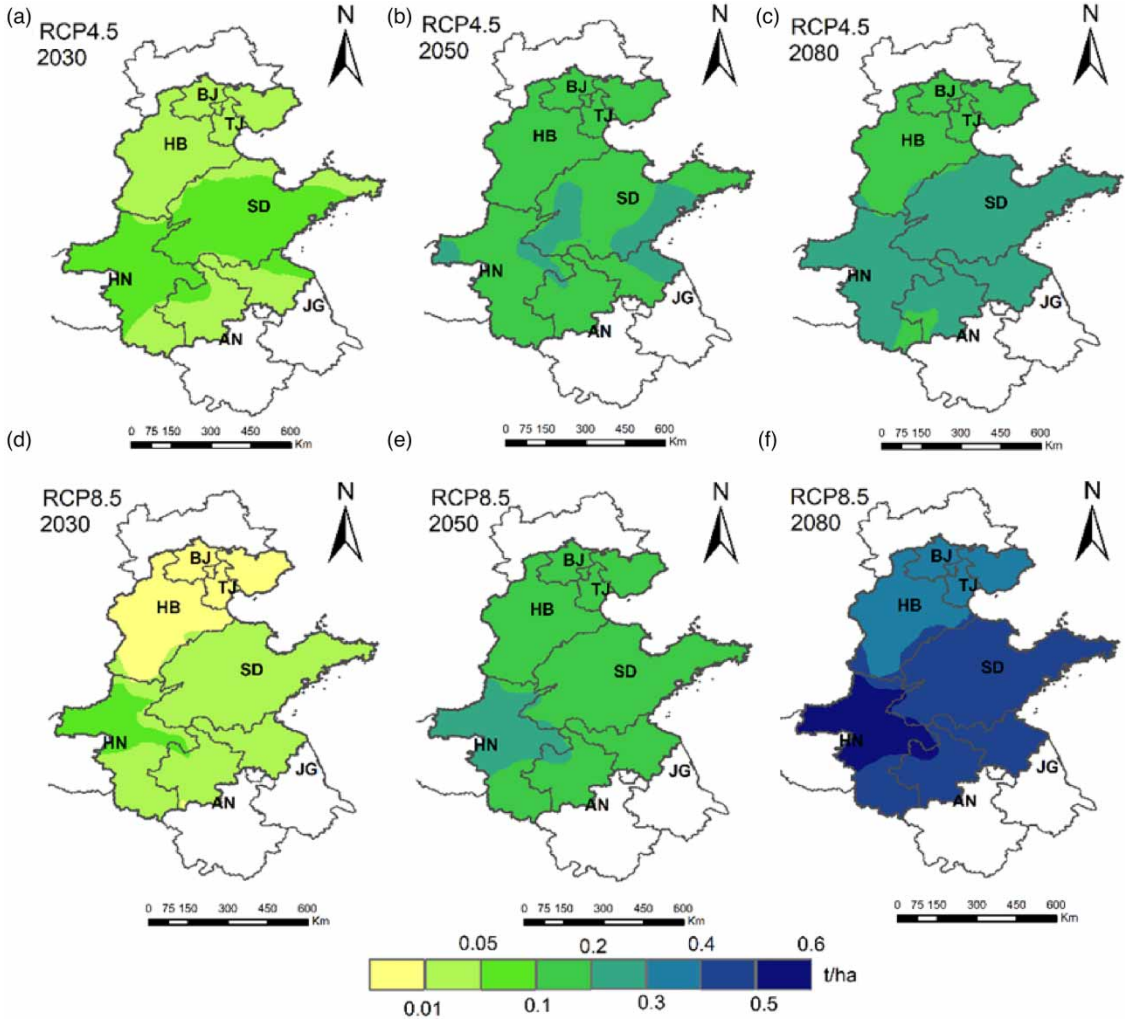

Figure 11 | Impact of climatic variables on winter wheat yield in the 2030s, 2050s, and 2080s under RCP4.5 (a–c) and RCP8.5 (d–f), respectively, relative to the base period.

between predictors and climate models is expected to improve the forecast results. Therefore, this study dealt with the uncertainty by evaluating the model performance using various evaluation methods and repeated the process several times to improve the model performance and reduce the bias.

Downscaled climate change predictions in this study show a systematic increase in mean temperature and precipitation during the growth period of both winter wheat and summer maize under all emission scenarios. The substantial increase in all climatic variables is projected during the summer MGP as compared to the winter WGP. According to Ding *et al.* (2007), under varied emission scenarios, China's average annual temperature projected increase is 1.5–2.1 °C by 2020, 2.3–3.3 °C by 2050, and 3.9–6.0 °C by 2100, and an increase of 10–12% in precipitation relative to the base period 1961–1990. It has also been analyzed that daily minimum temperature is projected to increase more rapidly than daily maximum temperature, leading to an increase in daily mean temperature. This will result in a greater likelihood of extreme events and can have detrimental effects on crop grain yield. Geng *et al.* (2019) projected an increase in precipitation in the 2060s during the winter WGP by 17.31 and 22.22% under RCP4.5 and RCP8.5 in the North China Plain (NCP) region, while our results show an increase of 1.33–4.17% under RCP4.5 and 3.13–8.61% under RCP8.5 for the period 2016–2099 for the winter wheat growing season. The reason can be due to variation in the selection of different study sites. In general, various statistical models indicate that northern China will have more precipitation in the future and significant warming during the 21st century (Ding *et al.* 2007). An increase in precipitation is thought to be beneficial for wheat and maize growth, reducing the

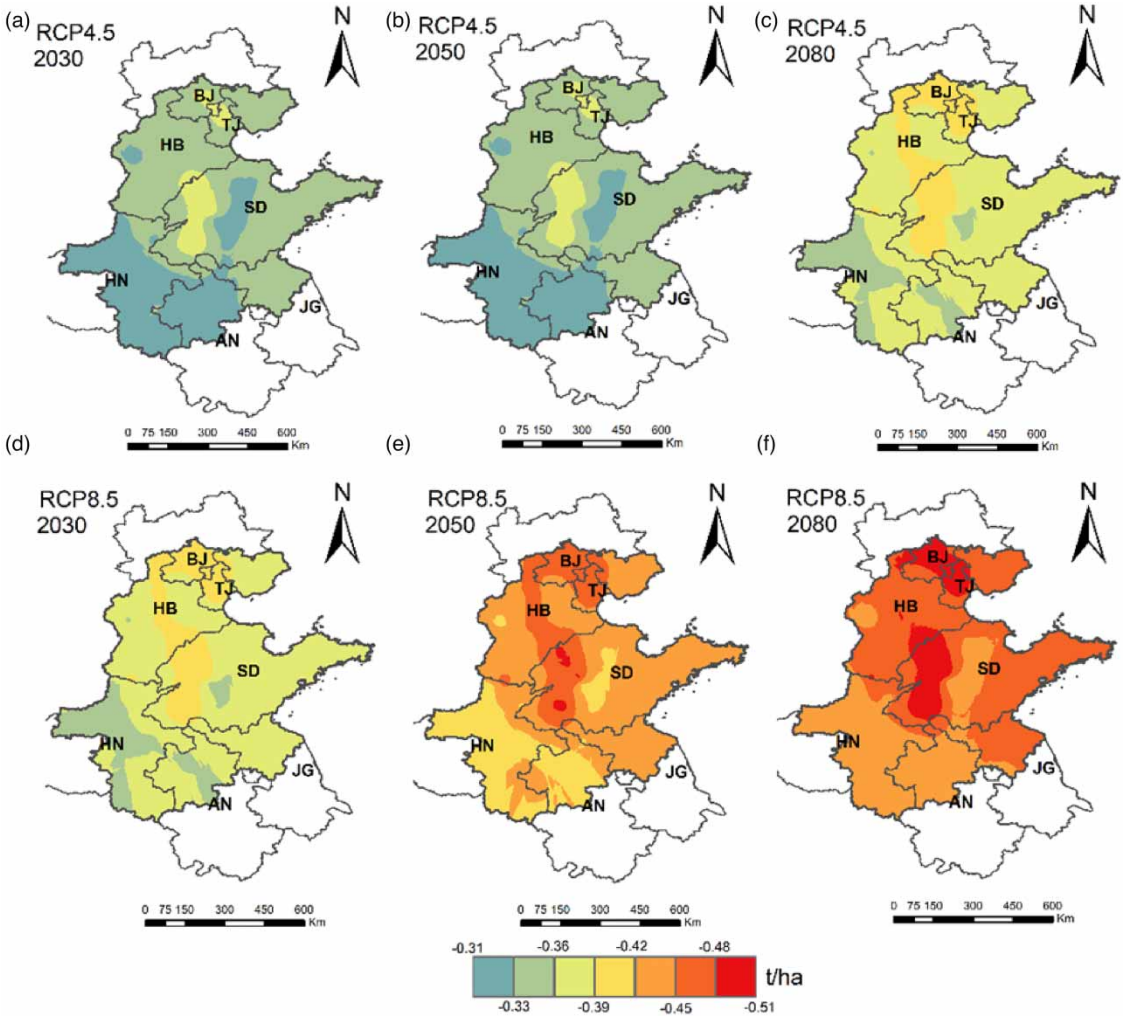

Figure 12 | Impact of climatic variables on summer maize yield in the 2030s, 2050s, and 2080s under RCP4.5 (a–c) and RCP8.5 (d–f), respectively, relative to the base period.

irrigation burden, but an increase in temperature can reduce the yield. Since the mid-1990s, increasing climate warming in the NCP has increased the probability of drought by an average of 10.1% (Hu *et al.* 2014). The warming trend will have a significant effect on drought occurrence in the summer MGP in the NCP region (Hu *et al.* 2014). Such changes can cause considerable changes in irrigation practices and grain yield for both of these crops in the NCP region.

The statistical models for China estimate that without climate adaptation, CO_2 fertilization, and genetic improvements in the crop cultivars, each degree-Celsius increase in global mean temperature will result in the loss of yield of $2.6 \pm 3.1\%$ for wheat and $-8.0 \pm 6.1\%$ for maize (Lobell & Field 2007). During the 1981–2016 period, in absolute terms, the contribution of climatic factors to winter wheat yield was estimated to be around 0.76–1.92%, while the contribution of technological advancements has been estimated to have a contributed 27.19–60.43% increase in agricultural yield (Geng *et al.* 2019), which indicates the effective adaptation strategies already in place. In the case of summer maize, Xiao *et al.* (2020) suggest that due to climate changes, maize yield will decrease in China by 2.3–2.4%, but water-use efficiency will increase by 11.8–26.6% if no adaptive strategy is put in place. In most cases, warm temperature increases the crop phonological development resulting in early senescence and reduced grain yield and biomass. The direct negative temperature impact on yield could be additionally affected via indirect temperature impacts. For instance, increasing temperature will increase atmospheric water demand, which could lead to additional water stress from increased water pressure deficits, subsequently reducing soil moisture and decreasing yield. It is also suggested that increased temperature impacts the evapotranspiration rate, leading to a

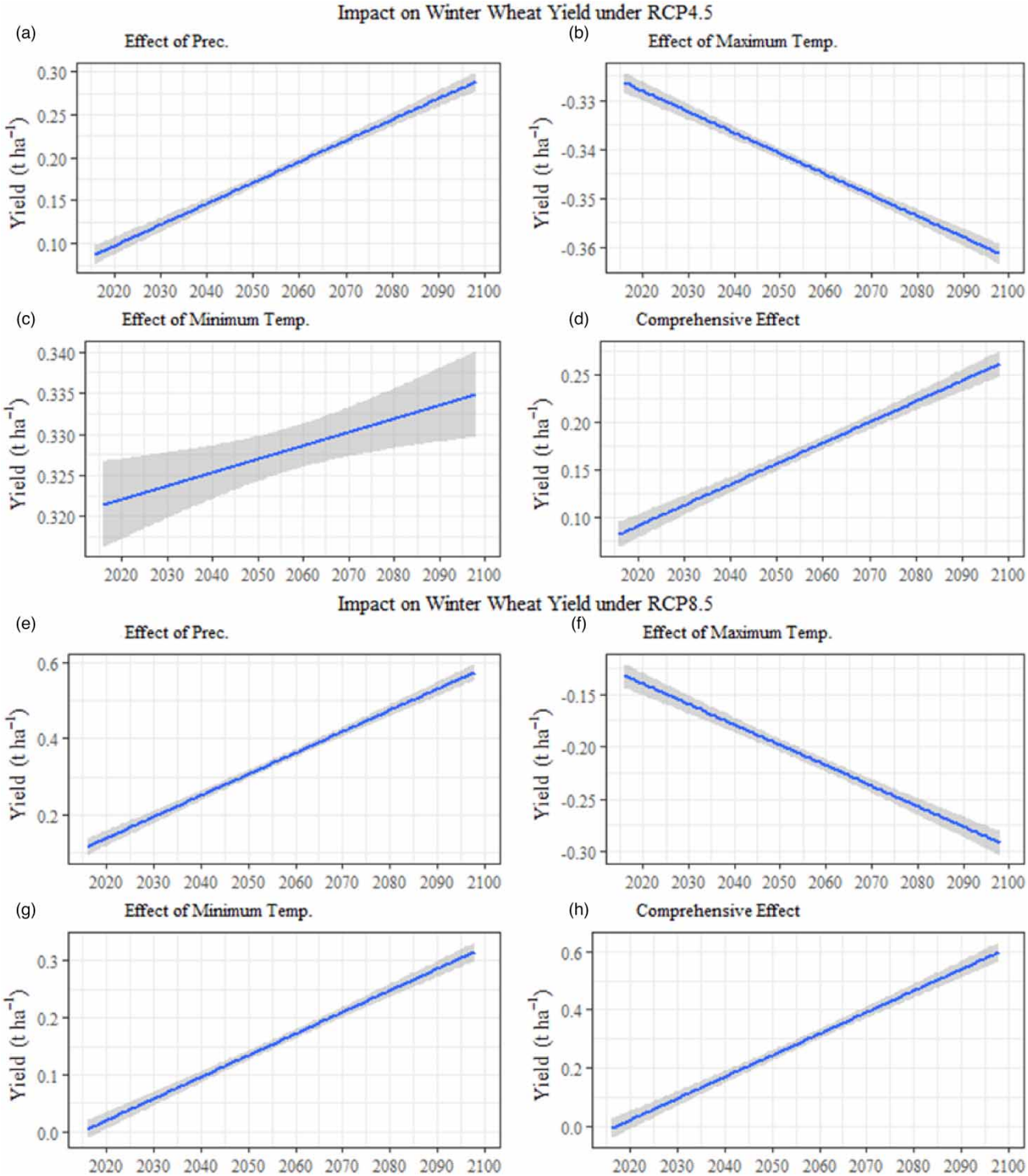

Figure 13 | Impact of climate change on winter wheat potential yield under RCP4.5 (a–d) and RCP8.5 (e–h).

faster loss in soil moisture and an increased need for irrigation. So, the areas that are likely to get wetter during summer in the MGP are also likely to experience temperature-driven drying.

The elevated temperatures are expected to accelerate the crop growth leading to shorter crop cycles (Salman *et al.* 2021). On the provincial scale, changes in climatic factors can vary from North to South in the NCP region which can have a varying effect on wheat yield. Geng *et al.* (2019) suggested that a 1% increase in mean temperature during the WGP can lead to a loss

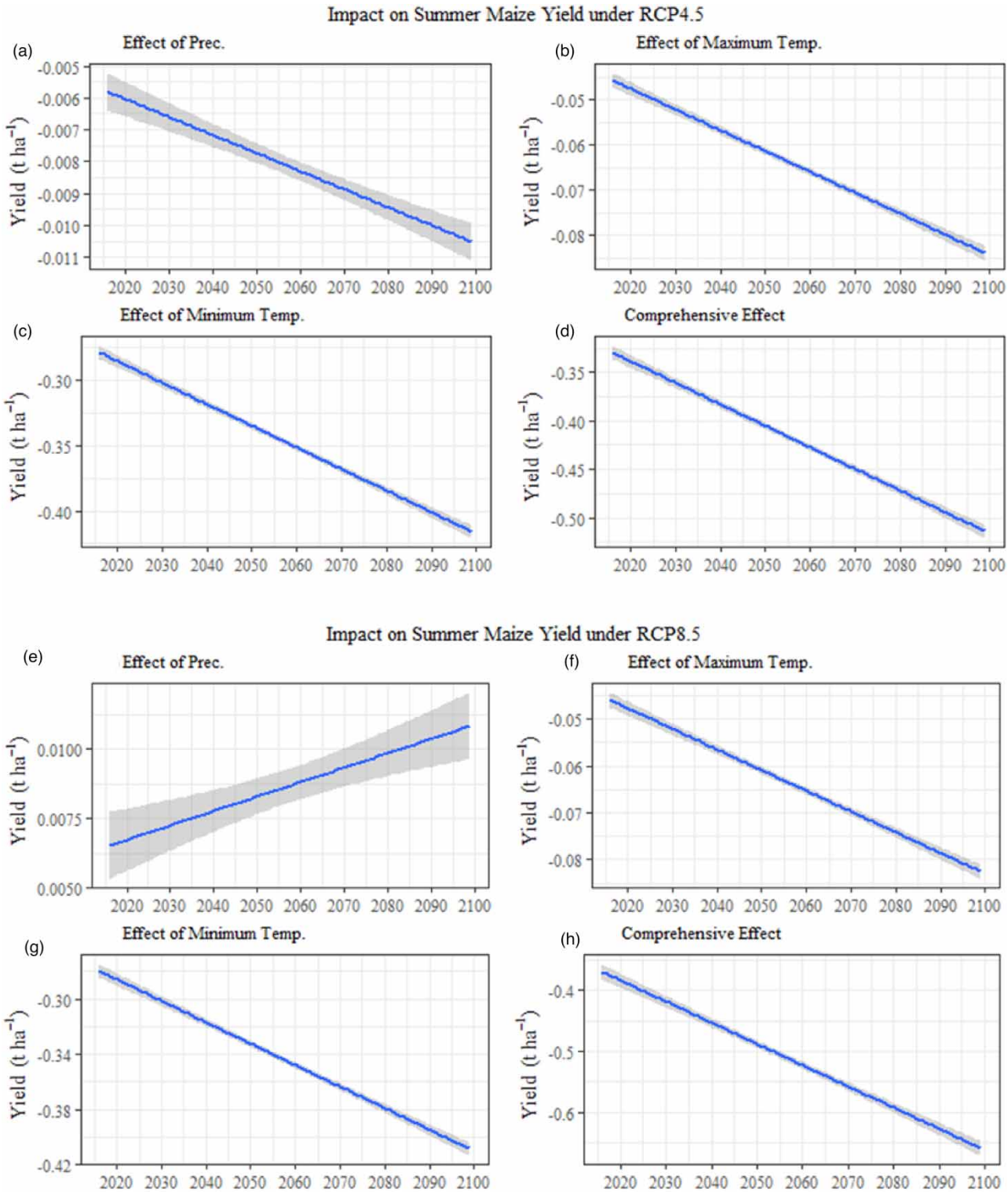

Figure 14 | Impact of climate change on summer maize potential yield under RCP4.5 (a–d) and RCP8.5 (e–h).

of 0.109% of winter wheat yield per unit area keeping other factors constant, and a 1% increase in precipitation will increase the wheat yield by 0.186% to a point where it becomes harmful (Geng *et al.* 2019). However, the cumulative effect of temperature and precipitation on winter wheat will be positive under RCP4.5 and RCP8.5 by 3.22 and 4.13%, respectively, for the

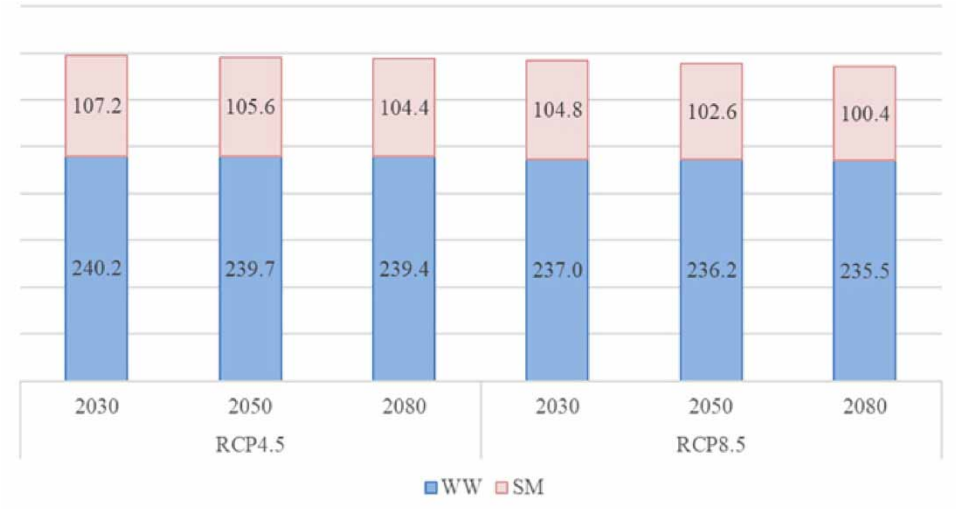

Figure 15 | Change in the length of winter wheat and summer maize growing seasons under RCP4.5 and RCP8.5.

period 2021–2050. The climatic factors will positively contribute to the winter wheat yield in the Jing–Jin–Ji region, Henan and Shandong. Our results also show similar spatiotemporal changes and much of the increase in wheat yield is concentrated in the central and south 3H region.

In another study, Tang *et al.* (2018) used the Decision Support System for Agrotechnology Transfer (DSSAT) model in the 3H Plain and estimated that the potential yield, crop water requirement (ET_c), and effective precipitation during winter wheat growing seasons might increase in the future under RCP4.5, while irrigation water requirements would decrease. The wheat and maize crop productivity has also been estimated in a study based on the potential crop evapotranspiration and water availability in the NCP. Under full irrigation when water demand is met, the wheat yield ranges from 6.9 to 10.2 t ha^{-1} and increases with latitude. Under rain-fed conditions, the wheat yield is much lower in all areas ranging from 0.6 to 5.2 t ha^{-1} and decreases in low-latitude areas due to decline in annual rainfall. Under full irrigation, the maize yield ranges from 9.2 to 13.6 t ha^{-1}, and under rain-fed conditions, it ranges from 6.1 to 13 t ha^{-1} with the lowest yield in the middle of the NCP due to the lowest amount of rainfall (Wang *et al.* 2008). This is consistent with the results of the current study where winter wheat yield increase is estimated largely in the central and lower 3H region, while summer maize yield is projected to decline in areas with reduced rainfall, mainly in north parts of the region.

The seasonality of the climatic changes also points toward the change in the length of crop cycles for both wheat and maize. The reduction of the wheat crop cycle from 242 days in the base period to 239 and 235 days under RCP4.5 and RCP8.5, respectively, indicates the effect of 1.71–1.28 °C warming. The summer maize crop length has declined substantially from 110 days in the base period to 104 and 100 days under RCP4.5 and RCP8.5, respectively. Liu *et al.* (2021) has also shown that the increase in accumulated thermal temperature will reduce the vegetative and reproductive growing period of wheat in the 3H Plain. Sharafati *et al.* (2022) have projected the impact of climate change on the variability of crop cycle length, crop yield, and water productivity in Iran. The results suggest an increase in wheat yield (14–54%), a decrease in the crop cycle length (1–12%), and an increase in water productivity (9–96%) in the future (2021–2080) as compared to the baseline period (1985–2016) (Sharafati *et al.* 2022).

In addition to temperature impacts, combined with the summer and autumn rainfall in the 3H region in the year 2021, the seasonal rainfall in the maize harvest period was too frequent and strong, resulting in floods and seriously affecting the maize production and also winter wheat sowing. According to the results of this study, the increase in precipitation may bring flood disaster risk while alleviating the contradiction of water shortage in agricultural production. The change in water budget during the winter WGP may not be very significant, but, during the summer MGP, it is expected to improve from 109 mm in the 2030s to 126 mm in the 2080s under RCP4.5 and 107 mm in the 2030s to 163 mm in the 2080s under RCP8.5 (Shirazi *et al.* 2022). The study of climate change impacts offers a good choice to change the cropping system for reducing the planting area of water-consuming crop (e.g. winter wheat) in those over-pumping areas to balance groundwater use and crop yield. The timely devised adaptive and mitigation strategies are the key to minimize the negative impacts of disasters on wheat and maize crops.

5. CONCLUSION

The study employed a crop simulation model combined with future climate data downscaled at 90 study locations across the 3H Plain to simulate changes in temperature and precipitation and their impact on wheat and maize yield and the cropping season within the region. The simulation results using the medium- and high-emission scenarios reveal that wheat and maize yield is sensitive to changes in temperature and precipitation. The projected climatic data indicate an increase in the average temperature throughout all RCP scenarios across the 3H Plain for both the winter WGP (1.17–1.21 °C under RCP4.5 and 1.17–1.28 °C under RCP8.5) and the summer MGP (1.29–1.92 °C under RCP4.5 and 1.84–2.08 °C under RCP8.5). The projected precipitation for both medium- and high-emission scenarios has been estimated to increase in the 2030s, 2050s, and 2080s during the WGP and the MGP. The comprehensive effect of an increase in all climatic variables will benefit wheat yield with an increase up to 1.74% (0.25 t ha^{-1}) and 3.00% (0.6 t ha^{-1}) under RCP4.5 and RCP8.5, respectively. The positive effect of the increase in climatic variables will increase gradually from the 2030s to the 2080s. It is likely that a substantial increase in precipitation will counteract the negative effect of rising temperatures during the winter WGP, particularly in Shandong and parts of Henan in comparison to other provinces. The northern areas of the 3H plain will have crop water requirements similar to present conditions, leading to slight variations in wheat yield. For summer maize, the comprehensive effect of all variables is projected to decrease the yield up to 4.44% (0.5 t ha^{-1}) and 5.40% (0.6 t ha^{-1}) under RCP4.5 and RCP8.5, respectively, by the end of this century. The loss of maize yield is much more pronounced in the north 3H region due to an increase in mean temperatures, despite any substantial change in precipitation. The highest decrease in maize yields was projected in the 2080s under both RCP scenarios. The effect of increased thermal temperature for both winter wheat and summer maize is projected to reduce the length of growth cycles in both vegetative and reproductive growing periods. The projected changes suggest that the enhanced efforts for adaptation and mitigation strategies such as adjustments in planting dates, cultivar improvements, enhanced soil fertility, better irrigation, and management practices are needed to minimize the climate change impacts on reference crops. This study only covered the use of single GCM, and future work could be extended to the use of multi-models or multi-model ensemble to generate future daily weather data. In addition, we only used a single crop model. The use of multiple crop models and their response to ensembled climate data can also reveal interesting findings.

ACKNOWLEDGEMENTS

This research was supported by the Joint Foundation between the National Science Foundation of China (NSFC) and the Consultative Group for International Agricultural Research (CGIAR) (No. C31661143011) and the Agricultural Science and Technology Innovation Program of CAAS 'Research on national food security strategy of China in the new era' (CAAS-ZDRW202012).

DATA AVAILABILITY STATEMENT

All relevant data are included in the paper or its Supplementary Information.

CONFLICT OF INTEREST

The authors declare there is no conflict.

REFERENCES

Bian, C., Ma, C., Liu, X., Gao, G., Liu, Q., Yan, Z., Ren, Y. & Li, Q. 2016 Responses of winter wheat yield and water use efficiency to irrigation frequency and planting pattern. *PLoS ONE* **11** (5), e0154673. doi:10.1371/journal.pone.0154673.

Chen, Z., Wang, H., Liu, X., Liu, Y., Gao, S. & Zhou, J. 2016 The effect of N fertilizer placement on the fate of urea-15N and yield of winter wheat in Southeast China. *PLoS ONE* **11** (4). doi:10.1371/journal.pone.0153701.

Ding, Y., Ren, G., Zhao, Z., Xu, Y., Luo, Y., Li, Q. & Zhang, J. 2007 Detection, causes and projection of climate change over China: an overview of recent progress. *Advances in Atmospheric Sciences* 954–971. doi:10.1007/s00376-007-0954-4.

Geng, X., Wang, F., Ren, W. & Hao, Z. 2019 Climate change impacts on winter wheat yield in Northern China. *Advances in Meteorology*. doi:10.1155/2019/2767018.

He, J., Yang, K., Tang, W., Lu, H., Qin, J., Chen, Y. & Li, X. 2020 The first high-resolution meteorological forcing dataset for land process studies over China. *Scientific Data* **7** (1), 25. doi:10.1038/s41597-020-0369-y.

Hu, Y., Liu, Y. & Li, Z. 2014 Impact of climate warming on drought characteristics of summer maize in North China Plain for 1961–2010. In: *The 3rd International Conference on Agro-Geoinformatics, Agro-Geoinformatics*. Institute of Electrical and Electronics Engineers, Inc. doi:10.1109/Agro-Geoinformatics.2014.6910598.

IPCC 2018 *Global Warming of 1.5 °C. An IPCC Special Report on the Impacts of Global Warming of 1.5 °C Above Pre-Industrial Levels and Related Global Greenhouse Gas Emission Pathways in the Context of Strengthening the Global Response to the Threat of Climate Change, Sustainable Development, and Efforts to Eradicate Poverty*. Intergovernmental Panel on Climate Change, Geneva, Switzerland.

IPCC 2019 Summary for policymakers. In: *Climate Change and Land: An IPCC Special Report on Climate Change, Desertification, Land Degradation, Sustainable Land Management, Food Security, and Greenhouse Gas Fluxes in Terrestrial Ecosystems* (Shukla, P. R., Skea, J., Calvo Buendia, E., Masson-Delmotte, V., Pörtner, H.-O., Roberts, D. C., Zhai, P., Slade, R., Connors, S., van Diemen, R., Ferrat, M., Haughey, E., Luz, S., Neogi, S., Pathak, M., Petzold, J., Portugal Pereira, J., Vyas, P., Huntley, E., Kissick, K., Belkacemi, M. & Malley, J., eds). Intergovernmental Panel on Climate Change, Geneva, Switzerland.

Jin, X., Feng, H., Zhu, X., Li, Z., Song, S., Song, X., Yang, G., Xu, X. & Guo, W. 2014 Assessment of the AquaCrop model for use in simulation of irrigated winter wheat canopy cover, biomass, and grain yield in the North China Plain. *PLoS ONE* **9** (1), e86938. doi:10.1371/journal.pone.0086938.

Li, X., Ju, H., Sarah, G., Yan, C., Batchelor, W. D. & Liu, Q. 2017 Spatiotemporal variation of drought characteristics in the Huang-Huai-Hai Plain, China under the climate change scenario. *Journal of Integrative Agriculture* **16** (10), 2308–2322. doi:10.1016/S2095-3119(16)61545-9.

Liu, Y., Chen, Q., Chen, J., Pan, T. & Ge, Q. 2021 Plausible changes in wheat-growing periods and grain yield in China triggered by future climate change under multiple scenarios and periods. *Quarterly Journal of the Royal Meteorological Society* **147** (741), 4371–4387. doi:10.1002/QJ.4184.

Lobell, D. B. & Field, C. B. 2007 Global scale climate-crop yield relationships and the impacts of recent warming. *Environmental Research Letters* **2** (1). doi:10.1088/1748-9326/2/1/014002.

Lv, S., Yang, X., Lin, X., Liu, Z., Zhao, J., Li, K., Mu, C., Chen, X., Chen, F. & Mi, G. 2015 Yield gap simulations using ten maize cultivars commonly planted in Northeast China during the past five decades. *Agricultural and Forest Meteorology* **205**, 1–10. doi:10.1016/j.agrformet.2015.02.008.

Motha, R. P. & Baier, W. 2005 Impacts of present and future climate change and climate variability on agriculture in the temperate regions: North America. *Climatic Change* **70** (1), 137–164. doi:10.1007/S10584-005-5940-1.

Rosenzweig, C., Elliott, J., Deryng, D., Ruane, A. C., Muller, C., Arneth, A., Boote, K. J., Folberth, C., Glotter, M., Khabarov, N., Neumann, K., Piontek, F., Pugh, T. A. M., Schmid, E., Stehfest, E., Yang, H. & Jones, J. W. 2014 Assessing agricultural risks of climate change in the 21st century in a global gridded crop model intercomparison. *Proceedings of the National Academy of Sciences of the United States of America* **111** (9), 3268–3273. doi:10.1073/PNAS.1222463110/SUPPL_FILE/SAPP.PDF.

Salman, S. A., Shahid, S., Sharafati, A., Salem, G. S. A., Bakar, A. A., Farooque, A. A., Chung, E. S., Ahmed, Y. A., Mikhail, B. & Yaseen, Z. M. 2021 Projection of agricultural water stress for climate change scenarios: a regional case study of Iraq. *Agriculture* **11** (12), 1288. doi:10.3390/AGRICULTURE11121288.

Sharafati, A., Tayyebi, M. M., Pezeshki, P. & Shahid, S. 2022 Uncertainty of climate change impact on crop characteristics: a case study of Moghan plain in Iran. *Theoretical and Applied Climatology*. doi:10.1007/s00704-022-04074-9.

Shirazi, S. Z., Mei, X., Liu, B. & Liu, Y. 2021 Assessment of the AquaCrop model under different irrigation scenarios in the North China Plain. *Agricultural Water Management* **257**, 107120. doi:10.1016/j.agwat.2021.107120.

Shirazi, S. Z., Mei, X., Liu, B. & Liu, Y. 2022 Estimating potential yield and change in water budget for wheat and maize across Huang-Huai-Hai Plain in the future. *Agricultural Water Management* **260**, 107282. doi:10.1016/j.agwat.2021.107282.

Tang, X., Song, N., Chen, Z., Wang, J. & He, J. 2018 Estimating the potential yield and ETc of winter wheat across Huang-Huai-Hai Plain in the future with the modified DSSAT model. *Scientific Reports* **8** (1), 1–12. doi:10.1038/s41598-018-32980-4.

Umair, M., Shen, Y., Qi, Y., Zhang, Y., Ahmad, A., Pei, H. & Liu, M. 2017 Evaluation of the CropSyst model during wheat-maize rotations on the North China Plain for identifying soil evaporation losses. *Frontiers in Plant Science* **8**, 1667. doi:10.3389/fpls.2017.01667.

Wang, E., Yu, Q., Wu, D. & Xia, J. 2008 Climate, agricultural production and hydrological balance in the North China Plain. *International Journal of Climatology* **28**, 1959–1970. doi:10.1002/joc.1677.

Wang, Y., Zhang, Y., Zhang, R., Li, J., Zhang, M., Zhou, S. & Wang, Z. 2018 Reduced irrigation increases the water use efficiency and productivity of winter wheat-summer maize rotation on the North China Plain. *Science of the Total Environment* **618** (2), 112–120. doi:10.1016/j.scitotenv.2017.10.284.

Xiao, D., Liu, D. L., Wang, B., Feng, P. & Waters, C. 2020 Designing high-yielding maize ideotypes to adapt changing climate in the North China Plain. *Agricultural Systems* **181**, 102805. doi:10.1016/j.agsy.2020.102805.

First received 3 January 2022; accepted in revised form 7 July 2022. Available online 19 July 2022